Final Draft
of the original manuscript:

Wagner, S.; Widmann, M.; Jones, J.; Haberzettl, T.; Luecke, A.; Mayr, C.; Ohlendorf, C.; Schaebitz, F.; Zolitschka, B.:

Transient simulations, empirical reconstructions and forcing mechanisms for the Mid-holocene hydrological climate in southern Patagonia

In: Climate Dynamics (2007) Springer

DOI: 10.1007/s00382-007-0229-x

Transient simulations, empirical reconstructions and forcing mechanisms for the Mid-Holocene hydrological climate in Southern Patagonia

Sebastian Wagner[1], **Martin Widmann**[1], **Julie Jones**[1], **Torsten Haberzettl**[2], **Andreas Lücke**[3], **Christoph Mayr**[3], **Christian Ohlendorf**[2], **Frank Schäbitz**[4] **and Bernd Zolitschka**[2]

January 10, 2007

[1] GKSS Research Centre, Institute for Coastal Research, Geesthacht, Germany

[2] Institute of Geography, University of Bremen, Bremen, Germany

[3] Institute of Chemistry and Dynamics of the Geosphere V, Research Centre Jülich, Jülich, Germany

[4] Seminar for Geography and its Didactics, University of Cologne, Cologne, Germany

Corresponding author: swagner@gkss.de, phone: ++49 4152 87 1862, fax: ++49 4152 87 1888, GKSS Research Centre, Max-Planck-Str.1, 21502 Geesthacht, Germany

Abstract

This study investigates the atmospheric circulation in transient climate simulations with a coupled atmosphere-ocean General Circulation Model (GCM) for the mid-Holocene (MH) period 7 ka BP–4.5 ka BP driven with combinations of orbital, solar and greenhouse gas forcings. The focus is on southern South America. Statistical downscaling models are derived from observational data and applied to the simulations to estimate precipitation in south-eastern Patagonia during the MH. These estimates are compared with lake level estimates for Laguna Potrok Aike (LPA) from sediments. Relative to pre-industrial conditions (i.e. 1550–1850), which show extraordinarily high lake levels, the proxy based reconstructed lake levels during the MH are lower. The downscaled simulated circulation differences indicate higher LPA precipitation during the MH from March to August, higher annual means, and reduced precipitation from September to February. Thus the reconstructed lower LPA lake levels can not be explained solely by the simulated precipitation changes. Possible reasons for this discrepancy are discussed. Based on proxy data from southern South America hypotheses have also been proposed on the latitudinal position of the Southern Hemispheric Westerlies (SHWs). In agreement with some of these hypotheses our simulations show an increased seasonal cycle of the latitudinal position of the SHWs during the MH, which can be explained by the orbital forcing. The simulations also show stronger SHWs over southern Patagonia during austral summer and weaker SHWs during winter. The downscaling model associates weaker SHWs with increased precipitation in the LPA region. However, this relationship is only moderate, and therefore the downscaling model does not support the assumption of a strong link between mean SHWs and precipitation over south-eastern Patagonia, which is the basis of many proxy-based hypotheses about the SHWs.

1 Introduction

In the Southern Hemisphere (SH) high latitudes only very few continental climate proxy data exist due to the large oceanic areas, and southern South America is the only non-ice covered continent extending into the high mid latitude SH. Proxy data from South America have the potential to allow reconstructions of the past SH climate, including its main atmospheric circulation feature, the Southern Hemispheric Westerlies (SHWs).

Different hypotheses on the latitudinal position and strength of the SHWs over southern South America during the mid-Holocene have been formulated in several studies. Lamy et al. (2001) analysed iron contents from a marine sediment core from the Chilean continental slope (approx. 41° S; 74° W) and reconstructed less humid conditions between 7.7 ka and 4 cal ka BP than in the late Holocene. As the SHWs transport moisture to western Chile, the authors conclude that during the mid-Holocene the SHWs were located in a more poleward position than in the late Holocene. After 4.0 cal ka BP conditions are reconstructed to be more humid in conjunction with a more northerly position of the SHWs. Holocene precipitation in Central Chile (33° S; 71° W) has been reconstructed by Jenny et al. (2003) from proxy data using a water balance model. Low precipitation was found for the early Holocene, followed by pronounced wet conditions during the mid-Holocene, which were attributed to a poleward deflection of the SHWs due to a strengthened Pacific subtropical high pressure cell in the mid-Holocene. Our analysis will concentrate on the SHWs over South America, as changes may differ regionally (cf. Wardle 2003).

Hypotheses about atmospheric circulation that are derived from proxy data are usually based on assumptions or conceptual models on the links between the large-scale atmospheric circula-

tion and precipitation, and between precipitation and lake conditions. With our study we want to contribute to an objective formulation of the former link by describing the relation between the monthly mean circulation over southern South America and precipitation in south-eastern Patagonia using statistical downscaling models fitted with recent climate observations. We also investigate whether mid-Holocene SHWs conditions estimated from proxy data can be found in transient simulations with a coupled atmosphere-ocean General Circulation Model (GCM) for the period 7 ka BP–4.5 ka BP, which are driven either by orbital, or by orbital, solar and greenhouse gas forcing. In addition, we use the statistical downscaling models to estimate precipitation in south-eastern Patagonia from the simulations and compare the estimates with lake level reconstructions for Laguna Potrok Aike from sediments. This is further motivated by the fact that a link between the SHWs and precipitation can be expected from known links between the Southern Hemisphere Annular Mode (SAM), which describes the strength of the SHWs, and precipitation over the Southern Hemisphere (Jones and Widmann 2003), for example over Australia (Meneghini et al. 2006), over southeastern South America (Silvestri and Vera 2003), and over western South Africa (Reason and Rouault 2005).

The estimation of local or regional precipitation from coarse-resolution GCM simulations by means of a statistical downscaling model addresses a fundamental problem encountered when comparing climate simulations and proxy data. Proxy data typically include signals of the local- or regional-scale climate. On these scales GCM simulations cannot be directly used for several reasons. Firstly, the low model resolution and the resulting poor representation of mountain ranges (e.g. the Andes) lead to unrealistically simulated mesoscale circulation features for a

given synoptic-scale atmospheric state. Secondly, even for a given synoptic- and mesoscale atmospheric state, precipitation is often not realistically simulated by coarse resolution GCMs, as was shown in reanalysis-based studies in which the first error type is small (e.g. Janowiak et al. 1998; Widmann and Bretherton 2000). The second error type is due to the fact that real-world precipitation involves processes on spatial scales much smaller than the model resolution, which are taken into account in the models through parametrisations. These parametrisations are far from perfect and can cause large errors on the grid-point scale. Sub-grid-point-scale variability of the true precipitation, which usually is large over complex topography and which can not be simulated, additionally contributes to the second error type.

One approach for estimating local or regional precipitation from GCM simulations is to use Perfect-Prog(nosis) statistical downscaling (e.g. von Storch et al. 1993; Matulla et al. 2002). It is based on statistical models that use large-scale atmospheric predictors to estimate the small scale predictands. These statistical models are derived from present-day empirical data and thus describe real-world relationships. As a consequence one needs to use predictors that are realistically simulated by the numerical model, hence the name Perfect-Prog. Numerical weather prediction often uses an alternative approach, the so-called Model Output Statistics (MOS), which attempts to correct systematic models errors and can be highly skilful. Unfortunately MOS-models are difficult to fit for the GCMs used in paleo-simulations (cf. Widmann et al. 2003), and therefore we will use a Perfect-Prog downscaling model to estimate precipitation in south-eastern Patagonia from the large-scale circulation in our mid-Holocene simulations.

It should be noted that statistical downscaling always assumes the stability of the statistical relationships through time. The validity of this assumption is very difficult to assess, and our results

should be seen as a first step towards providing simulation-based mid-Holocene precipitation estimates for south-eastern Patagonia, and as a test whether precipitation estimates based on this assumption lead to an agreement between downscaled climate simulations and lake level proxies.

Coarse-resolution climate simulations can also be compared with large-scale climate features estimated from local proxy data by means of some type of 'upscaling'. The aforementioned proxy-based hypotheses on mid-Holocene circulation are examples for the (implicit) use of upscaling relationships that are derived from meteorological considerations, while many temperature and circulation reconstructions for the late-Holocene use objective statistical relationships, which have been derived in the instrumental period (cf. Mann et al. 1999; Jones and Widmann 2003; Luterbacher et al. 2004). Although our study does not explicitly formulate upscaling models, the backward interpretations of our downscaling models provide one type of several mathematically plausible upscaling models and can be compared to the upscaling relationships implicitly used for the proxy-based circulation studies.

Simulations of the mid-Holocene climate have also been conducted by other groups. Quasi-equilibrium simulations with atmospheric GCMs for 6 ka BP with prescribed constant orbital and solar forcing, SSTs and greenhouse gas concentrations have been performed for instance in the framework of the Paleoclimate Model Intercomparison Project (PMIP) (e.g. Masson et al. 1999; Bonfils et al. 2004). Brown et al. (2006) analysed the amplitude, frequency and phase of ENSO in quasi-equilibrium GCM simulations for the mid-Holocene and compared them with coral records. To our knowledge our simulation is the first transient standard simulation for

the mid-Holocene with an atmosphere-ocean GCM. Earlier transient GCM simulations that include the mid-Holocene have so far been performed with accelerated orbital forcing (Lorenz and Lohmann 2004; Hall et al. 2005), which reduces the number of actually simulated timesteps for a given period and focusses on the atmospheric response (therefore Hall et al. 2005 use a slab ocean). Mikolajewicz et al. (2003) undertook 1000 year long quasi-equilibrium simulations for 6 ka BP with a coupled atmosphere-ocean general circulation model and compared the results with uncoupled simulations. The authors point to the importance of the coupling because of an intensification of the climate signal in the monsoon system and a warming of high northern latitudes. A number of Holocene simulations have also been carried out with models of intermediate complexity (e.g. Ganopolski et al. 1998; Claussen et al. 1999; Weber et al. 2004; Renssen et al. 2005). However, none of these simulations has been analysed with a focus on southern South America.

One aim of our study is to investigate the strength of the simulated SHWs to orbital forcing. We are not aware of earlier model studies of this question that focus on the mid-Holocene. However, there are several publications that analyse the SHWs in quasi-equilibrium GCM simulations for the Last Glacial Maximum (LGM). For instance Wyrwoll et al. (2000) find a latitudinal extension, intensification and poleward movement of the zonal mean SHWs over South America during the LGM southern winter relative to modern conditions, which is attributed to reduced temperatures and increased sea ice cover around Antarctica. Wardle (2003) finds similar simulated LGM SHWs and compares them with proxy-based SHWs reconstructions from southern Australia. A systematic statistical analysis of the northern hemispheric circulation response to orbital forcing and of the dynamical mechanisms has been conducted by Hall et al. (2005). The

authors used a GCM simulation with accelerated forcing for the last 165 ka and found a strong response of the northern annular mode during northern winter. Thus, all of these studies suggest a noticeable circulation response to orbital forcing.

A problem investigating the SHWs is their somewhat unclear definition. This holds true for both proxy and modelling studies. For example in model-based studies Wardle (2003) considers the statistics of anticyclone system density and strength to infer the position of the SHWs, whereas Wyrwoll et al. (2000) consider a number of measures including zonal mean zonal winds, the eady growth rate parameter and high-pass transient eddy heat flux. In this paper we define the SHWs in terms of the location and strength of the extratropical, maximum zonal winds over South America along 70° W at the 850 hPa level. We want however to acknowledge that changes of the SHWs over South America can not directly be assigned to the entire SH. A more thorough discussion of this issue is given in Section 5.3.

The paper is structured as follows: The next section introduces the proxy site in south-eastern Patagonia and climatic hypothesis based on the proxy data in that region. Section 3 describes the climate model, the experimental setup and the data sets we use for the statistical downscaling. Section 4 contains the downscaling procedure. In section 5 the model results will be presented including a discussion of possible driving mechanisms of the zonal winds during the mid-Holocene. Results are summarised and discussed in section 6.

2 Proxy data and related hypotheses in south-eastern Patagonia

The regional focus of the following analysis is the Laguna Potrok Aike (LPA; 52° S, 70° W) which is located in the Pali Aike volcanic field in south-eastern Patagonia. Here information contained in the sediment cores of the crater lake LPA has been analysed with respect to changes of lake levels. The lake level changes at LPA are mainly controlled by the interplay of regional precipitation and evaporation. This is due to the small catchment area (200 km^2) of the lake. A surface runoff into the crater lake only occurs episodically through a few canyons during the snow-smelt in spring. Westerly winds are prevailing during 50% of the time (Haberzettl et al. 2005). Instrumental observational meteorological data at LPA are only available for the last six years. According to these data yearly mean precipitation ranges between 150 and 300 mm. The mean temperature is about 5.8 °C (unpublished data, G. Oliva, pers. comm.). Longer records of monthly precipitation are available from Rio Gallegos airport, 90 km east of the LPA.

Changes of the lake level at LPA are reflected by the sedimentary proxy indicators total inorganic carbon content (TIC) and the oxygen isotopic composition of lacustrine carbonates ($\delta^{18}O$carb). A reduction of the lake's water volume as a response to a negative hydrological balance leads to an increasing concentration of dissolved solids. This in turn causes the precipitation of lake internal carbonate (TIC) if a certain threshold is passed. When the lake level falls below the threshold when all the carbonate has been precipitated, TIC can no longer be used as a proxy. Therefore precipitation of TIC reacts non-linearly to changes in the hydrological

balance. A reduction of the lake volume leads also to higher $\delta^{18}O$carb values in the precipitated carbonates due to evaporative heavy isotope enrichment of the lake water (e.g. Li et al. 1997). The observed wide range of isotope values clearly indicate that temperature-dependent isotope fractionation (e.g. Teranes et al. 1999) played a minor role.

The average values of both proxies during the mid-Holocene period (4.5 to 7.0 ka BP) clearly indicate lake levels that have been lower than during the pre-industrial period, i.e. 1550–1850 (Fig. 1). It should be noted that the pre-industrial period 1550–1850 was exceptional in terms of a lake level high stand at LPA that is unprecedented in the entire Holocene. The reason for the lower lake levels during the mid-Holocene is a negative hydrological balance, for which potential causes are reduced precipitation, higher evaporation, higher air temperatures or higher wind speeds, or a combination thereof.

A short sediment core from LPA has been studied by Haberzettl et al. (2005) in terms of climatically induced lake level changes during the last two millenia. Here TIC also was used as a proxy for lake level changes. Lake levels were also reconstructed to have been lower during the late middle Ages and the 20th century compared to the Little Ice Age. A similar climatic course during the last millennium was reconstructed from a multi-proxy study of sediment cores from Laguna Azul about 60 km WSW of LPA (Mayr et al. 2005).

Paleoclimate studies in the vicinity of LPA have also been undertaken by Markgraf et al. (2003) for Lago Cardiel, 330 km to the north of LPA. For the mid-Holocene around 6 ka BP lake levels are reconstructed to have been generally lower but with repeated fluctuations. These fluctuations are not evident at LPA. This might point to latitudinal differences in the hydrological climate within a few hundred kilometres.

Concerning the driving mechanisms of the lake level variations at Lago Cardiel, Markgraf et al. (2003) argue that a shift within the position of the stormtracks controls the moisture transport into south-eastern Patagonia. The more northerly position of the SHWs stormtracks to the north of 50° S during the early Holocene they suggest allows Antarctic cold fronts to advect moisture from the South Atlantic in the East into southern Patagonia. During the late Holocene the stormtracks shifted seasonally with an overall more meridional, i.e. a south-north oriented behaviour. These shifts in the position resulted in less and more variable moisture due to the season-dependent position of the stormtracks. This result confirms the hypotheses of a former study carried out by Markgraf (1993) based on palynological records in southern Patagonia. Here it is concluded that the modern situation with a pronounced seasonal shift in the position of SHWs has not been established before 4.5 ka BP. In a most recent paper, Gilli et al. (2005b) propose increased activity of the SHWs during the mid-Holocene. The authors draw their conclusions also on sedimentological and petrophysical analysis of cores form Lago Cardiel. It is hypothesised that the strengthening is possibly caused by an increase in the temperature gradient as a result of enhanced influence and/or southward migration of the southeast Pacific anticyclone and a larger Antarctic sea-ice extent.

For the mid-Holocene, especially after 6 ka BP, pollen and sediment records in south-eastern Patagonia are interpreted by Schäbitz (1999) and Mancini et al. (2005) as indications for higher seasonal variations in the latitudinal positions of the SHWs compared to the present. This hypothesis is also based on the assumption that the hydrological signal in the proxy data is mainly controlled by the easterly advection of humid air masses from the south Atlantic into south-eastern Patagonia.

The previously introduced studies formulate qualitative assumptions on the links between the large-scale atmospheric circulation (SHWs) and the local hydrological climate in south-eastern Patagonia. The aims of the paper in this respect are i) to understand the mechanisms linking the local hydrological regime in terms of precipitation in south-eastern Patagonia with the large-scale atmospheric circulation and ii) to investigate on the strength of these relationships (cf. section 4).

3 Model description and Experimental Setup

The model we use for the transient simulations of the mid-Holocene is the coupled atmosphere-ocean general circulation model ECHO-G (Legutke and Voss 1999). It consists of the atmospheric part ECHAM4 (Roeckner et al. 1996) and the oceanic part HOPE-G (Wolff et al. 1997). Both sub-models have been developed at the Max Planck Institute of Meteorology in Hamburg. The atmospheric model has a horizontal resolution of T30 (approx. 3.75° lat x 3.75° lon) and 19 vertical levels. The ocean model HOPE-G has an effective horizontal resolution of approximately 2.8° lat x 2.8° lon with 20 vertical levels, five of them between 200 and 10 hPa. In the tropical regions a grid refinement is employed with decreasing meridional grid-point distance. This increased resolution reaches a value of 0.5° at the equator and should allow for a more realistic representation of ENSO events. The climate model is adjusted for freshwater and heat fluxes in order to avoid climate drift. The flux adjustment, which has to be calculated from observational data, is held constant in time and has no annual cycle. Since the flux-adjustment is derived from observational data and not sufficient information is available to estimate it for other time periods. Therefore it is the same in all simulations. Although Brown et al. (2006) use

a non-flux adjusted model in their time-slice experiments, for the mid-Holocene to our knowledge no multi-centennial simulations with non flux-corrected AOGCMs have been carried out until now. Long transient simulations without flux correction could however help to assess the influence of the flux correction on time scales of centuries. Without these non-flux corrected simulations one can only speculate on the potential effects, e.g. in terms of oceanic sea ice or atmosphere-ocean heat exchanges in high latitudes and oceanic regions influenced by the El-Niño Southern Oscillation.

The present experimental setup includes two forced simulations for the mid-Holocene. Both have been initialised at the end of a 500 year spin-down control (quasi-equilibrium) run with constant (orbital, solar and greenhouse gas) forcing for 7 ka BP. The reference experiment is a 300 year long control simulation with constant pre-industrial forcing (hereafter denoted as 'CONPRE').

The first experiment, in the following denoted as 'ORB' (Orbital), is carried out using only variations in the orbital forcing between 7 ka BP and 4.5 ka BP (Berger and Loutre 1991). The solar constant has been set to a value of 1365 Wm^{-2} and the greenhouse gas concentrations to 280 ppm (CO_2), 700 ppb (CH_4) and 265 ppb (N_2O), respectively.

Figure 2 shows the differences in insolation due to orbital forcing between different times of the mid-Holocene (7 ka BP, 6 ka BP, and 5 ka BP) and the present-day values. The SH shows a negative insolation anomaly during summer (DJF) in the low latitudes and tropics extending into the high latitudes. In winter (JJA) the differences are positive over the tropics. In the course of the mid-Holocene the amplitude of the insolation differences decreases.

The second experiment, in the following denoted as 'ORBSG' (Orbital, Solar and Greenhouse-gas), is carried out using additional variable solar and greenhouse gas forcing. The solar forcing was estimated by scaling production estimates of $\Delta\,^{14}C$ (cf. Solanki et al. (2004)) such that the difference between present-day and Maunder Minimum solar activity is 0.3% (Crowley 2000) (Fig. 3, upper panel). This value is well within the range of different solar reconstructions (Bard et al. 2000).

The greenhouse gas concentrations are deduced from air trapped in Antarctic ice cores and have been provided by Flückiger et al. (2002) (Fig. 3, lower panel). Due to the high uncertainty involved in the reconstruction of the volcanic activity during the time of the mid-Holocene, this forcing was not included into this experiment. All experiments have been carried out with fixed prescribed (pre-industrial) vegetation.

The ECHO-G model has been used with constant stratospheric ozone distribution. A number of papers have addressed the importance of the interactions between ozone and the incoming solar radiation. For example, Fröhlich and Lean (2004) state that the variations in the solar output are most pronounced in the short wavelengths controlling the creation and destruction of stratospheric ozone. However, for a proper simulation of ozone dynamics a higher resolved stratosphere would be necessary. Therefore Lean et al. (2005) propose to extend the upper boundary of GCMs even above the stratosphere and using spectrally resolved rather than total irradiance variations. For the time of the mid-Holocene spectrally resolved information on solar irradiance is however not available.

The absorption of shortwave radiation by stratospheric ozone also has implications on tropo-

spheric temperatures and circulation. Rind et al. (2004) conclude that stratospheric temperature changes related to stratospheric ozone dynamics lead to a negative phase of the AO during the Maunder Minimum. Thompson et al. (2005) analyzed stratosphere-troposphere coupling in the Southern Hemisphere and found that changes in the stratospheric polar vortex precede anomalies in the SH annular mode (SAM), which in turn lead to changes in surface temperatures over large parts of Antarctica. Because of the lack of a dynamical ozone module in ECHO-G the ozone-related effects on tropospheric temperatures and circulation can not be captured by our model simulations.

Sea ice cover is interactively calculated with a sea ice model. No mid-Holocene sea ice initial conditions have been prescribed. Instead, we assume that during the 500 year spin-down simulation the sea ice has adapted to mid-Holocene conditions at 7 ka BP. The importance of oceanic sea ice for the synoptic variability in the circum-Antarctic regions has been highlighted by several authors (e.g. Carleton 1983; Simmonds and Wu 1993; Watkins and Simmonds 1995). For example, Simmonds and Wu (1993) find in their sensitivity study with a GCM more cyclones in the sea ice-free Weddell and Ross Seas. The changes in cyclogenesis are however mainly restricted to a latitudinal band centered over the Antarctic coast. We will not provide a detailed analysis of the oceanic sea ice variability here, since our focus is much further to the north. It will also be shown later in the paper that most of the changes concerning the SHWs in the mid-Holocene are linked to changes in the upper troposphere.

The present-day atmospheric data that will be used for the establishment of relationships between circulation and precipitation at LPA are provided by the Climate Diagnostics Center

(CDC). To investigate the large scale atmospheric circulation we use the NCEP/NCAR-reanalysis data (Kistler et al. 2001). These data were obtained using a state-of-the-art analysis/forecast system to perform data assimilation using past data from 1948 to the present. The spatial resolution is 2.5° lat x 2.5° lon. It has been interpolated on the ECHO-G grid with 3.75° lat x 3.75° lon. The large scale atmospheric fields have been extracted for the region 90° W–40° W and 35° S–70° S. The precipitation data stem from the VASCLIMO project for the period 1951–2000 (Beck et al. 2004). The precipitation data have been quality checked and were interpolated onto different grid resolutions. Here the 0.5° grid has been used for analysis. The precipitation for the downscaling will be taken for the grid point corresponding to LPA. Additionally, station data from the World Meteorological Organisation (http://dss.ucar.edu/datasets/ds570.0/) have been used to calculate the relation between a simple circulation index and precipitation at Rio Gallegos.

4 Downscaling of the large-scale circulation

In order to investigate the links between the large-scale circulation and local precipitation we use a two-step strategy: In the first step we show that a connection between local precipitation and circulation is already evident using a simple circulation index. In the second step we set up a statistical downscaling scheme including regression models that we then apply to the simulated large-scale circulation of the mid-Holocene.

Since the reanalysis data can deviate from observational data, especially prior to the mid-1970s, we use in a first step instrumental station data to test whether a circulation-precipitation con-

nection is evident. A sea level pressure (SLP)-index has been calculated and correlated with precipitation in south-eastern Patagonia. The stations entering this index are Argentine Island at 65.30° S; 64.30° W and Puerto Madryn at 43.30° S; 65.40° W. For precipitation we use monthly observations from the Rio Gallegos international airport. Fig. 4 shows the location of the stations together with the location of the city of Rio Gallegos and LPA.

The SLP index will be called South American Zonal Index (SAZI) and it has been defined as the normalised monthly pressure difference between Puerto Madryn and Argentine Island. High SAZI values indicate a pronounced westerly circulation, negative indices a reduced westerly circulation. The zero line indicates the mean westerly flow. Since the data at Argentine Island only extend from 1958 to 1982 the analysis is based on this time interval.

The histogram of monthly precipitation at Rio Gallegos (not shown) reveals that the data are not normally distributed. Therefore the data have been log-transformed prior to the analysis.

Fig. 5 shows the evolution of the SAZI pressure index together with the log-transformed precipitation time series at Rio Gallegos for DJF and JJA, respectively. The linear correlation coefficient between the two time series is -0.41 (DJF) and -0.56 (JJA). Thus, a positive index is related to negative precipitation anomalies and vice versa. Dynamically, this implies that a reduction in the intensity of the westerly winds is associated with positive precipitation anomalies at Rio Gallegos.

As already mentioned in the introduction, the climate model we use has a quite coarse resolution and therefore the simulated local-scale variables, such as precipitation, cannot directly be used over the complex terrain of southern South America. Using the original climate model precipitation output would lead to false conclusions about the connection between precipitation and

the large-scale circulation. To obtain more reliable results the large-scale simulated fields have to be downscaled. Afterwards the results for the local scale can be expected to be more reliable since e.g. the lee-effect of the Andes mountains that is important for the climate in south-eastern Patagonia is included implicitly in the downscaling model because the models were calibrated with observational data. The following section introduces the downscaling methodology that will be applied to the model simulations in the next sections.

For the large-scale atmospheric data set the NCEP/NCAR reanalysis data will be used (Kistler et al. 2001). The correlation between the NCEP-SAZI and the station-based SAZI is about r$\sim$+0.8 for JJA. During DJF the correlation is lower around r$\sim$+0.6. This point might be of specific importance when estimating the performance of the downscaling models, since the NCEP data show discrepancies to the observational record (for further discussion refer e.g. to Simmonds and Keay 2000, and Bromwich and Fogt 2004). Unfortunately, due to the shortness of the observational pressure data ending in 1982, we cannot estimate whether the correlations between the station-based SAZI and the NCEP SAZI improve in the period between 1981–2000. Furthermore the NCEP-data show trends in the leading SLP-PCs, which are most pronounced during DJF (cf. Thompson et al. 2000). As it is not a priori clear that these trends are related to precipitation trends, we take a prudent approach for estimating the regression coefficients that link the SLP PCs to VASCLIMO precipitation, and detrend all data prior to determining the downscaling model. This ensures that the regression coefficients are not influenced by the trends. The final downscaled precipitation for the mid-Holocene is obtained by applying this downscaling model to predictors that have not been detrended. For comparison we have also fitted downscaling models without detrending and obtained similar results for the downscaled

precipitation. From the VASCLIMO gridded precipitation data set (Beck et al. 2004) we selected the grid point that is closest to LPA. An advantage of the VASCLIMO data set is that it comprises another ten years of quality-controlled data.

For downscaling we use principal component regression (PCR), in which standard multiple linear regression (MLR) is applied to a subset of the leading principal components (PCs) of the predictor field (cf. Luterbacher et al. 2002). We have tested several combinations of large-scale predictor fields (SLP, geopotential height, zonal and meridional wind, relative humidity) and have obtained the best results for the model validation using SLP and 500 hPa zonal wind (U500) as large-scale predictors.

Using PCR, the predictor PCs can either be calculated separately for the two fields, or the principal component analysis (PCA) can be performed for the combination of the two fields (after the fields have been subjected to an overall scaling that ensures identical total variance in the two components). The model performs best with predictor PCs from separate PCAs. However, in this model setup the leading PCs of SLP and U500 are highly correlated ($r \sim +0.8$). Due to this co-linearity the regression models are not robust and the regression coefficients cannot be physically interpreted. The physical plausibility of the regression models is, however, of specific importance, since we want to apply the statistical relationships in a climate supposedly different from present-day conditions. Therefore we decided to use only the leading PCs of the SLP-field as predictors in our final model. Since the PCs entering the regression models are not correlated, the regression coefficients are independent and as a consequence the final regression weights for the SLP fields, which will be shown below, are also dynamically consistent.

Our multiple regression model can be written as

$$APREC_{log}(t) = a_0 + \sum_{k=1}^{K} a_k^{SLP} pc_k^{SLP}(t) + \epsilon(t) \quad (1)$$

where $APREC_{log}(t)$ are the log-transformed precipitation anomalies, a_k are the regression coefficients and $pc_k^{SLP(t)}$ are the predictor PCs. a_0 is zero in our case since we use precipitation anomalies. The index k runs from 1 to the number of predictors K. We use the leading 5 PCs of the SLP fields that explain approx. 90% of the total variance. Retaining this number of EOFs does not violate the North et al. (1982)-test, i.e. with our selection we do not truncate pairs or multiplets of degenerated EOFs. ϵ(t) are the residuals that can not linearly be explained by the regression model. We formulate the models separately for every season on a monthly basis.

The skill of the downscaling model has been assessed through cross-validation. Here we use a modified leave-one-out method (cf. Michaelson 1997) in which we estimate precipitation for one month based on a statistical model that is fitted using all months with the exception of a 5 month window centred around the month to be estimated. We leave more than one month out to account for the weak temporal autocorrelation in the predictor PCs. This technique does however not completely solve the memory problem, but in most cases the autocorrelation falls to values below 0.1 after two months. Furthermore, applying this procedure, the month to be predicted is always separated by one year from the months used for calibration.

All estimated months are finally concatenated and then compared to the true precipitation. As skill measures we use the Pearson correlation between estimates and the true precipitation, the root mean square errors (RMSE) and the reduction of error (RE, e.g. Cook et al. 1994). The

RE compares the RMSE of the downscaling model with the RMSE of a no-knowledge estimate, which is here chosen to be the climatological mean. The range of RE values is between $-\infty$ and 1. Values of 1 indicate perfect reconstruction, values around 0 indicate that the reconstructions are as good as the climatological mean and negative values indicate reconstructions worse than using the climatological mean. All three skill measures are shown in Table 1, along with the correlation for the fitting period with all months between 1951 and 2000 included. The correlations are based on the log-transformed precipitation and are statistically significant at the 1% level for all seasons in the calibration and validation period. The RE values and the RMSE are estimated on the basis of the absolute precipitation values in the verification period.

In general the performance of the models is quite low with highest correlations in the validation period in JJA. The latter can possibly be explained by the more vigourous circulation during southern hemispheric winter over southern South America in the model and the stronger connection between the large-scale circulation and precipitation. The downscaling model for summer (DJF) shows very unsatisfactorily results for the validation period, since only 6% of the variance in the validation period can be explained. One reason for the weak performance of the models might be related to processes controlling precipitation that act on the sub-monthly timescale, e.g. in terms of short-lived circulation anomalies that are not captured in the monthly mean large-scale circulation fields. However, it could also be that precipitation is influenced by processes independent to the atmospheric circulation (e.g. soil moisture content, SSTs in the South Atlantic). A further reason might pertain to the quality of the NCEP/NCAR reanalysis data in the time prior to 1979. The cross-validation based on the period 1979–2000 does, however, not lead to an improvement of the model skill. Furthermore it should be noted that the

skill measures refer to the performance of the models at interannual time scales. Therefore the question arises to what extent these skill measures are valid also for the decadal or centennial variability.

The precipitation estimates in Eq. 1 are expressed as linear combinations of the PCs, because this is how the statistical model is originally formulated. Since the PCs are defined as the orthogonal projection of the anomaly field onto the EOFs, the estimated precipitation can be expressed equivalently as a weighted mean of the original grid-cell data. The weight patterns are given by the sum of the EOFs weighted with the MLR regression coefficients a_k^{SLP}. This representation of the downscaling model is well suited for investigating the physical plausibility of the statistical downscaling model. When too many PCs are used in our downscaling model the weight patterns appear meteorologically implausible. This is due to the fact that the higher EOFs are multipole patterns which often do not represent dynamically consistent large-scale circulation anomalies, or which capture circulation teleconnections that are misleading when applied in the downscaling context. Although including higher PCs may slightly improve the fitting and validation statistics of the downscaling model, we emphasise physical plausibility when selecting the final model, as this increases the chance that the downscaling model can be applied in a meaningful way during the mid-Holocene. We thus use only a few leading PCs which are mostly connected with physically plausible EOFs. However, the leading EOFs can still include circulation teleconnections, which needs to be taken into account when interpreting the weight patterns over regions that are far away from the Laguna Potrok Aike region.

The SLP regression weight patterns are shown in Fig. 6. They can be interpreted analogously to

circulation anomalies, because SLP anomalies that have a spatial structure similar to the weight pattern will lead to positive precipitation estimates, and similarly shaped circulation anomalies with the opposite sign will lead to negative precipitation anomalies.

For DJF, the SLP pattern (Fig. 6, left panel) shows negative anomalies over the Pacific off the western coast of Chile in conjunction with a latitudinal band of positive anomalies around 60° S. The JJA pattern (Fig. 6, right panel) is similar to DJF. However, the center of the negative pole is located over the Atlantic ocean and the positive anomalies are centred south of South America. Hence both circulation patterns show a blocking-like structure reducing the strength of the westerly circulation over southern Patagonia. The negative anomalies south of the Antarctic Peninsula are possibly an artefact of the downscaling model. To sum up, positive precipitation anomalies at LPA are associated with weaker westerly winds and vice versa. These are evident in the blocking-like SLP weight patterns for both DJF and JJA. These results are also consistent with results obtained from the analysis of the SAZI and precipitation at Rio Gallegos.

5 Model Results

5.1 Precipitation at LPA during the mid-Holocene

To investigate precipitation at LPA during the mid-Holocene, a downscaling of the simulated large-scale circulation is carried out using the results obtained in the previous section. As already mentioned in the introduction, an a priori shortcoming of this approach is the assumption that circulation-precipitation connections have been constant over time back to the mid-Holocene. In this respect Villalba et al. (1998) conclude, based on the analysis of tree-ring data in northern Patagonia, that the influence of high-latitude circulation on precipitation appears to

be more significant during the twentieth century compared to previous times. However, we have made the assumption that the dynamical links between atmospheric circulation and precipitation at LPA have been similar during the mid-Holocene. Furthermore, as discussed in the last section, we only included a few physical meaningful predictors in the statistical model in order to reduce the uncertainty related to the robustness of the transfer functions.

The regression coefficients from the MLR analysis for the period 1951–2000 have been used to downscale the large-scale atmospheric SLP fields. The simulated PCs have been used as predictors. They have been calculated by projecting the ECHO-G anomalies onto the NCEP/NCAR SLP EOFs. The anomalies were obtained by subtracting the climatological mean of the pre-industrial control simulation from the ORB and ORBSG simulation. Thus, the resulting precipitation time series show differences with respect to the pre-industrial climate. It should be noted here that the downscaled precipitation changes are related only to circulation changes and not changes caused by background thermal changes due to insolation changes. However, as will be shown in the next section some of the thermal changes caused by orbital forcing are included implicitly through internal climate feedbacks.

Figures 7 and 8 show the estimated precipitation at LPA for ORB and ORBSG for DJF and JJA, respectively, obtained by downscaling the simulated large-scale SLP. The zero line refers to the pre-industrial mean. The time series have been smoothed with a 30 year Hamming window. Additionally the confidence intervals are given. These were estimated on the basis of the standard deviations of the observed precipitation residuals (=standard errors). Since a filter has been applied on the estimated precipitation time series, the reduction of variance has been

taken into account by dividing the respective twofold standard errors (corresponding to the 95% confidence intervals) by $\sqrt{n}$, with n being the length of the filter window. The use of $\sqrt{n}$ is justified, because seasonal precipitation at interannual timescales shows autocorrelations close to zero.

For DJF (upper panels of Figs. 7 and 8) the ORB simulation shows a slight, albeit non-significant, reduction in precipitation. The ORBSG simulation additionally shows a slight negative trend that is not evident in the ORB simulation. The confidence intervals show a quite wide range due to the weak performance of the downscaling model in DJF.

During JJA (middle panels of Figs. 7 and 8) both mid-Holocene simulations show in general increased precipitation with respect to the pre-industrial control simulation. Furthermore a positive trend is evident in both simulations.

The annual situation (lower panels of Figs. 7 and 8) shows slightly increased precipitation. Here the ORB simulation shows a positive trend possibly induced by the increase in JJA precipitation, whereas the opposite trends in DJF and JJA in the ORBSG simulation cancel each other out. (The annual precipitation anomalies are calculated on basis of all four seasons; MAM and SON have not been shown). To investigate mean precipitation changes, Table 2 shows the differences with respect to the pre-industrial control simulation together with the significance of the differences for the different seasons and the annual mean. The estimation of the significance is also based on uncertainties related to the observed twofold standard errors of the regression models. Accordingly, during DJF and SON mean precipitation is lower than in CONPRE, whereas during MAM and JJA it is significantly higher. On an annual basis the estimated mean precipitation is also slightly, albeit statistically non-significant, increased. It is important to note that the sign

of the differences remains unchanged for all seasons, irrespective of the additional solar and greenhouse-gas forcing included in ORBSG.

Based on our analysis that considers precipitation to be the major driver of lake level changes at LPA, the model results are inconsistent with the results based on the proxy data that indicate lower lake levels compared to the pre-industrial period 1550–1850 (cf. Section 2). As previously discussed, lake level changes are the result of the interplay between precipitation (P) and evaporation (E). In the semi-arid climate of south-eastern Patagonia it is important to take also into account changes of P-E to compare results with the reconstructed lake levels on a consistent basis. However, since it is not possible to downscale the large-scale circulation on evaporation as no observational data are available, the model results cannot capture the full range of lake level changes. Therefore it is possible that the changes in E might result in P-E being consistent with the reconstructed lake levels.

Furthermore also a change in the thermal background characteristics might have a profound influence on evaporation and precipitation and hence on lake level changes. These thermal changes are not captured by our downscaling method, since no temperature-sensitive predictors enter into the regression models. Apart from those physical reasons another explanation for the deviations between the model and the proxy data pertains to the large uncertainties involved in the statistical downscaling procedure (cf. confidence intervals in Figs. 7 and 8). Additionally, also uncertainties associated with the proxy data have to be taken into account. Therefore, these sources of uncertainty complicate the reconstruction of the local hydrological regime at LPA.

5.2 Circulation changes over South America during the mid-Holocene

As local precipitation at LPA is estimated by downscaling of regional-scale SLP, in this section we investigate firstly how the regional mean SLP differs between the mid-Holocene (ORB simulation) and the pre-industrial climate (CONPRE simulation), and secondly how these differences change through time, by analysing the SLP trends.

The mean differences for SLP between ORB and CONPRE are shown in Fig. 9. The DJF-SLP pattern (Fig. 9, upper left) shows reduced pressure south of 50° S. According to the regression weight pattern (Fig. 6) this results in reduced precipitation at LPA in ORB, as is seen in the downscaled precipitation time series (Figure 7). This result is also consistent with the modelled ORB-SAZI (not shown), which shows an increased pressure gradient during the mid-Holocene, favouring reduced precipitation at LPA.

During JJA the situation is different. The mean SLP (Fig. 9, upper right) shows increased pressure southwest of southern South America with maximum differences around 60° S, resulting in reduced pressure gradients, as is also evident from the modelled SAZI of the ORB simulation. This pattern is also consistent with the estimated increase in precipitation at LPA. It is important to note that these circulation changes are also evident in higher tropospheric layers, e.g. for the zonal winds at the 850 hPa level. This level will be used in the next section for the analysis of changes in the position of the SHWs in the model simulations. Therefore it is already noted here that there exists a close relation between changes in the SLP field and changes in the zonal winds at the 850 hPa level.

The lower panel of Fig. 9 shows the linear trends of the SLP fields. Only statistically significant

values at the 5% level are given. The significance has been estimated on the basis of a linear regression analysis. The DJF-SLP pattern (Fig. 9, lower left) shows a negative trend south of 60° S, which could be expected to result in a precipitation decrease. However the downscaled precipitation time series shows no indication of such a trend. Thus, the trend south of 60° S is possibly too weak or remote to exert an influence on the precipitation at LPA. In JJA the pattern is again quite different, with negative SLP trends in the northwest of the domain between 35° S and 40° S and positive trends between 50° S and 70° S with maximum values around 50° W and 65° S (Fig. 9, lower right). This results in increased precipitation in the course of the mid-Holocene during JJA, as is seen in the precipitation time series of Fig. 7.

5.3 Simulated position of the southern hemispheric zonal winds along 70° W

The previous section considered the regional pressure changes and their relationship to precipitation changes over southern South America. This section, and section 5.4, consider the larger-scale circulation changes in the context of the SHWs, as it is changes in these that proxy studies such e.g. of Markgraf (1993) and Schäbitz (1999) have drawn their conclusions. Note that this paper mainly focuses on the SHWs over South America, as changes in the westerlies may differ in other regions (Wyrwoll et al. 2000). As already mentioned in the introduction we want to annotate that the regional diagnosis of the SHWs over South America do not necessarily reflect conditions over the entire SH. In Section 5.4. we therefore also consider horizontally zonal winds over the SH.

To investigate possible changes in the position of the simulated zonal winds over southern South America we analyse the location and strength of the simulated maximum zonal wind velocities (MZWs) along 70° W over the SH, at different tropospheric levels (200, 500 and 850 hPa). A number of diagnostics of the SHWs could be used (e.g. Wyrwoll et al. 2000). We chose this relatively simple index because more complex analysis is beyond the scope of this paper.

In the following we restrict the definition of the SHWs to the 850 hPa level. This is motivated by the fact that we wanted i) to exclude wind influencing processes related to surface conditions and ii) to distinguish the extratropical westerlies in the lower troposphere from the southern jet streams in the upper troposphere. Therefore we expect that the zonal winds at the 850 hPa level reflect best changes related to the extratropical westerlies, on which the aforementioned proxy hypotheses are drawn.

The evolution in the MZWs at the different tropospheric layers is given in Figure 10. In DJF the simulated MZWs show a more poleward position compared to the pre-industrial simulation at all levels. The latitudinal differences are mostly pronounced at the 200 hPa level (Figure 10, left panel). In both simulations the decadal to centennial variability dominates the millennial-scale variability and no clear long-term trends can be determined except for the 850 hPa level for ORBSG. Here the poleward deflection does not occur before 6250 BP. During JJA (Fig. 10, right panel) the MZWs in the ORB and ORBSG simulation show more equatorward positions compared to CONPRE at all levels. However, a poleward trend at the 200 hPa level is evident only in the ORBSG simulation.

The results for the mean position and intensity of the MZWs are summarised in Table 3 for the CONPRE, ORB and ORBSG simulations. During DJF a significant poleward deflection

is evident at all levels, except for the 850 hPa level in the ORBSG simulation, because of the more equatorward position until 6250 BP (cf. Fig. 10). The intensity of the MZWs is also significantly increased with the exception of the 200 hPa level showing reduced intensities. In contrast to DJF during JJA all levels show a significantly more equatorward position together with mostly significantly increased MZWs. Thus it can be concluded that the model simulation indicates intensified seasonal variations in the position and the intensity of the SHWs during the mid-Holocene. The following section will investigate the vertical and hemispheric-scale extent of these changes.

5.4 Vertical and hemispheric analysis of southern hemispheric zonal winds

To investigate the changes in zonal winds identified in Section 5.3, in this section we consider the vertical circulation along along 70° W and the hemispheric circulation at different levels. Before looking at the differences in the mean flow between the mid-Holocene and pre-industrial simulation, we first consider the mean flow in the CONPRE simulation.

The simulated mean zonal flow along 70° W is shown in the upper panel of Fig. 11 for the pre-industrial simulation for DJF (left panel) and JJA (right panel). The model reproduces well the known double jet structure in JJA (the low latitude subtropical jet (STJ) and the high latitude polar frontal jet (PFJ)) and the single jet structure (PFJ) in DJF (cf. Trenberth 1987; Hurrell et al. 1998). The middle and lower panels show also that the model correctly captures the larger latitudinal extension of the zonal winds in austral winter than in austral summer (Hurrell et al. 1998). However the model does not capture the fact that below 200 hPa in some areas of the

SH the westerlies are stronger in summer than in winter (Trenberth 1982; Hurrell et al. 1998), although over southern Patagonia at around 50° S higher winds are evident in this season.

The upper panel of Fig. 12 shows differences of the zonal winds for the ORB simulation for 6 ka BP–5.7 ka BP and the pre-industrial control simulation for DJF (left panel) and JJA (right panel). During DJF a tripole pattern with increased zonal winds between 0° S and 10° S in the upper troposphere and between 45° S and 60° S in the whole troposphere is evident. Winds are markedly reduced mainly in the upper troposphere between 15° S and 40° S. Thus, during DJF the PFJ moves southwards, together with a southward movement of the westerlies, resulting in an increase in westerly winds (cf. also Fig. 9 upper right). This pattern is also evident in the middle and lower left panel of Fig. 12, which clearly shows that the pattern also applies to other longitudes over the SH. At the 850 hPa level the differences in the extratropical SHWs are not as pronounced, but still are discernible.

The JJA pattern is markedly different to DJF. It shows a tripole pattern but with maximum negative wind anomalies at 200 hPa centred around 5° S and 50° S and positive wind anomalies around 30° S. The STJ has intensified and become more focused in the regions between 20° S and 40° S. It is the movement in this jet that is shown in the changes in maximum wind speed at the 200 hPa level. The PFJ, however, is more strongly linked to surface westerlies (Nakamura and Shimpo 2004). The STJ strengthening is greatest over the Pacific and South America, and is weaker over the Atlantic and Indian Oceans, and further north over the Australian sector.

5.5 Links between zonal winds and meridional temperature gradients

Westerly flow in the SH is thought to dominantly be maintained by feedback between transient eddies and the zonal flow (Lorenz and Hartmann 2001). The source of the eddy activity is related to instability associated with the lower tropospheric temperature gradient of mid-latitudes. More recent analysis suggests also an oscillatory feedback between medium frequency eddies and the zonal flow (Rashid and Simmonds 2004). Thus the structure of the simulated meridional temperature gradient, which is investigated in this section, may be expected to be related to changes in the zonal winds.

The upper panels of Fig. 13 show the differences of the tropospheric temperature gradients along 70° W between ORB (6 ka BP–5.7 ka BP) and CONPRE for DJF and JJA, respectively. In DJF the temperature gradients are increased over the southern parts of South America between 40° S and 60° S in the middle atmosphere up to a level of 200 hPa and decreased over the central parts between 20° S and 35° S. This pattern is evident over most of the SH. The increased low latitude temperature gradients may be related to the strengthening of the STJ, which is driven by differential heating between the tropics and the subtropics (Lorenz and Hartmann 2001), although the SH STJ has also been found to be related to the activity of the Asian summer monsoon (cf. Nakamura and Shimpo 2004 and references therein).

During JJA temperature gradients are increased over the central parts of South America between 15° S and 35° S extending into the upper troposphere, but reduced over the southern parts between 45° S and 70° S. The lower right panel of Fig. 13 showing the situation for the entire

SH is also consistent with the profile along 70° W. Hence the STJ strengthens, whereas the PFJ and the surface westerlies weaken due to reduced temperature gradients.

The changes of the temperature gradients could possibly be explained by changes in the orbital forcing, since the only difference between the ORB and CONPRE simulation are the differences in the orbital configuration. Thus, due to the increased equator-to-pole insolation gradient in JJA there is an increased low latitude meridional temperature gradient. However, it is also possible that the increased heating over North America has strengthened the STJ over South America (Yang and Webster 1990). The reduced temperature gradient at low latitudes in DJF may also be related to the reduced insolation gradient in this season.

To sum up, insolation differences due to changes in the orbital forcing exert an influence on the intensity and position of the zonal winds via changes in meridional temperature gradients. In the region of southern Patagonia, however, the situation is counter-intuitive since here the zonal westerly winds are increased during DJF and reduced during JJA. An interesting result concerning the differences in the wind velocities is the therefore non-uniform sign of the response with respect to latitude. Due to the latitudinal movement of the zonal winds some regions experience reduced wind velocities, whereas others show increased velocities. This point emphasises the need for regional resolved analysis in order to detect the different effects of changes caused by the external forcing on the atmospheric circulation.

Concerning the influence of the solar activity on the zonal winds differences between periods of increased and reduced solar activity have been analysed. Results suggest that changes in the solar activity also modify the intensity and position of the zonal winds. However, the amplitude of the differences is markedly weaker compared to changes induced by the orbital forcing.

6 Discussion and Conclusions

This study investigated the hydrological regime in south-eastern Patagonia during the mid-Holocene. Information from both proxy data and from transient simulations with the general circulation model ECHO-G were analysed. To close the gap between the large-scale climate variability represented by the simulation and the local-scale climate signal in the proxy data a statistical downscaling was applied to estimate precipitation in south-eastern Patagonia. The climate simulations also allowed comprehensive analysis of atmospheric circulation changes, in particular with respect to the SHWs.

For the mid-Holocene a number of proxy studies formulated hypotheses on potential changes of the SHWs over South America (cf. Markgraf 1993; Schäbitz 1999; Lamy et al. 2001; Jenny et al. 2003; Markgraf et al. 2003; Mancini et al. 2005; Gilli et al. 2005a; Gilli et al. 2005b). These hypotheses were usually derived in a two step process. In a first step proxy indicators from sediment cores, for instance total inorganic carbon (TIC) (i) or pollen data (ii) were used to reconstruct the paleoenvironmental state in terms of lake levels (i) or the distribution of paleovegetation (ii). Based on these reconstructions inferences on the large-scale circulation in terms of the SHWs were made in a second step. This second step is in general based on qualitative conceptual models on the link between the local environmental state and large-scale winds. The lack of sufficient instrumental meteorological records and the potential differences between modern and past climate make it in general difficult to derive these relationships from an empirical basis. Therefore it is often implicitly assumed that variations in the proxy record can be explained to a large extent by changes in the westerly winds. As a consequence of

the limited empirical knowledge there is for instance no agreement on whether precipitation changes are related to changes in the position or in the intensity of the SHWs or to both. It should be noted that the answer can depend on the season and on the location.

We therefore followed a quantitative approach to investigate the characteristics and also the strength of the circulation-precipitation relationship in south-eastern Patagonia. In the observational data we found a negative correlation between the strength of the near-surface winds and precipitation in south-eastern Patagonia. The strength of this relationship is in most cases only moderate on a monthly basis. Correlations are highest in JJA, where the strength of the westerly winds explains approx. 25% of the precipitation variability. Thus, in general our results confirm the dynamical processes that have already been qualitatively proposed by Markgraf (1993) and Markgraf et al. (2003). However, the fact that we found only a moderately strong circulation-precipitation link does not support the hypothesis of a pronounced link between zonal winds and precipitation in south-eastern Patagonia that is often assumed in the context of proxy-reconstructions.

Despite its limited strength we used this link to establish statistical downscaling models and applied them to estimate precipitation in south-eastern Patagonia from circulation differences between transient climate simulations of the mid-Holocene and a equilibrium simulation for the pre-industrial period. When selecting the downscaling model, emphasis was given on physical plausibility since it was used in a climate presumably different from the climate of the fitting period.

The precipitation in the mid-Holocene estimated with downscaling models calibrated in the second half of the 20th century is higher during March to August and lower during September to

February compared to the pre-industrial period. The reduced DJF precipitation estimates are due to increased near-surface westerly winds, the increased JJA precipitation is the result of reduced westerly winds. Precipitation is also slightly increased on an annual basis. The differences of the estimated precipitation are similar in both the ORB and ORBSG simulation. This implies that the additional solar and greenhouse gas forcing in ORBSG does not substantially affect the mean precipitation differences. In the course of the mid-Holocene there are, however, distinct differences between the ORB and ORBSG simulation at decadal time scales.

Under the assumption of precipitation-driven lake levels at LPA, the higher annual precipitation estimates obtained from the downscaled simulations appear inconsistent with the lower lake level reconstructions during the mid-Holocene at LPA compared to pre-industrial conditions. Assuming that the simulated circulation response to the orbital forcing and the reconstructed lake levels are realistic, this leaves different possibilities:

- Lake level changes are the result of a combination of precipitation variability and wind- or temperature-driven evaporation variability, and as a consequence our precipitation estimates can not fully explain lake level changes at LPA during the mid-Holocene.

- The mid-Holocene precipitation in the LPA region may not be explicable by differences in the circulation. This would be consistent with the fact that the connection between monthly mean circulation and precipitation is only moderate. The statistical description for the circulation-precipitation link could possibly be improved by formulating downscaling models on a daily rather than monthly basis, in order to account for synoptic-scale processes. However, this analysis would be strongly restricted by the short observational evidence on a daily basis.

- The link between mean circulation and precipitation may also be such that it can not be well

captured by a linear statistical model.

- The relationship between precipitation and circulation, which was derived from recent data and assumed to be constant through time may have changed.

As already mentioned, changes in the paleoenvironment have been used to derive hypotheses on the position of the SHWs over South America. Schäbitz (1999) and Mancini et al. (2005) suggested an increased seasonality of the SHWs at 6 ka BP compared to modern conditions. In contrast, Markgraf (1993) and Markgraf et al. (2003) concluded that modern conditions with a pronounced seasonality were not established before 4.5 ka BP. Gilli et al. (2005b) propose an increased strength of the SHWs during the mid-Holocene. In this respect our simulations indicate a stronger seasonal variability of the SHWs throughout the whole mid-Holocene from 7 ka BP until 4.5 ka BP compared to preindustrial conditions, and thus do not support the hypothesis formulated in Markgraf (1993) and Markgraf et al. (2003). The hypothesis of Gilli et al. (2005a) is only partly consistent with our simulations since stronger SHWs are only evident during DJF and SON (not shown), whereas during JJA and MAM (not shown) the SHWs are reduced. This result points towards the importance of seasonal differences in the strength and position of the SHWs during the mid-Holocene compared to pre-industrial conditions.

We have also investigated the vertical structure and hemispheric pattern of the zonal winds. It was shown that the ECHO-G model is able to reproduce the basic features of the southern circulation, including the subtropical and polar front jet streams (cf. Lorenz and Hartmann 2001; Hurrell et al. 1998). The simulated large-scale response of the atmospheric circulation to orbital forcing is consistent with former studies that find similar responses (cf. Wyrwoll et al. 2000;

Hall et al. 2005). The basic patterns of orbitally induced changes in atmospheric circulation for the mid-Holocene are characterised by an narrowing and intensification of the southern subtropical jet during JJA and an extension and reduction in the intensity of the jet during DJF. Since our analysis focused on changes of the SHWs over southern South America these results cannot directly be translated on the entire SH. The analysis for the entire SH does however indicate that the basic structure holds true, especially during DJF. In JJA, the changes in the SHWs are also longitude dependent, as found also by Wardle (2003) for the LGM.

Regarding the driving mechanisms, the circulation response can possibly be explained through changes in the tropospheric meridional temperature gradients caused by the orbital forcing. Regions with increased zonal winds are related to regions with increased meridional temperature gradients. The poleward located regions are however characterised by different conditions. In JJA, for example, the increased zonal winds and meridional temperature gradients in the subtropical jet are associated with reduced zonal winds over southern South America and reduced gradients in the polar frontal jet. As a consequence the extratropical westerlies over southern Patagonia are weaker during the mid-Holocene despite a more intense upper tropospheric southern jet stream. This demonstrates the latitude-dependent response of the atmospheric circulation to changes in the orbital forcing and emphasises the need for a regionally resolved analysis.

Acknowledgements. We would like to thank the two anonymous reviewers for their very valuable comments on the manuscript. We thank F. Kaspar and S. Lorenz for their help with the climate model, B. Kromer and J. Flückiger for providing the solar and greenhouse gas forc-

ing time series, respectively. Observational data were provided by the NOAA-CIRES Climate Diagnostics Center, Boulder, Colorado, USA, from their Web site at http://www.cdc.noaa.gov/. The climate simulation was carried out on a NEC SX-6 at the German Climate Computing Center (DKRZ). The work has been funded by the Federal Ministry of Education (BMBF) in the framework of the projects SALSA (01 LD 0034/35) and MIDHOL (01 ILD 0301).

References

Bard E, Raisbeck G, Yiou F, Jouzel J (2000) Solar irradiance during the last 1200 years based on cosmogenic nuclides. Tellus 52B:985–992

Beck C, Grieser J, Rudolf B (2004) A new monthly precipitation climatology for the global land areas for the period 1951 to 2000. Tech. Rep. 18, Global Precipitation Climatology Centre c/o Deutscher Wetterdienst

Berger A, Loutre MF (1991) Insolation values for the climate of the last 10 million years. Quaternary Sci Rev 10:29–317

Bonfils C, de Noblet-Ducoudré N, Guiot J, Bartlein P (2004) Some mechanisms of mid-Holocene climate change in Europe, inferred from comparing PMIP models to data. Clim Dynam 23:79–98

Bromwich DH, Fogt RL (2004) Strong trends in the skill of the ERA-40 and NCEP-NCAR reanalyses in the high and midlatitudes of the southern hemisphere, 1958–2001. J Clim 17:4603–4619

Brown J, Collins M, Tudhope A (2006) Coupled model simulations of mid-Holocene ENSO and comparisons with coral oxygen isotope records. Adv Geosci 6:29–33

Carleton A (1983) Variations in Antarctic sea ice conditions and relationships with Southern Hemisphere cyclonic activity, winters 1973–77. Archives for Meteorology, Geophysics, and Bioclimatology 32:1–22

Claussen M, Kubatzki C, Brovkin V, Ganopolski A, Hoelzmann P, Pachur H (1999) Simulation of an abrupt change in Saharan vegetation in the mid-Holocene. Geophys Res Lett 26:2037–2040

Cook E, Briffa K, Jones P (1994) Spatial regression methods in dendroclimatology: a review and comparison of two techniques. Int J Climatol 14:379–402

Crowley T (2000) Causes of climate change over the past 1000 years. Science 289:270–277

Flückiger J, Monnin E, Stauffer B, Schwander J, Stocker T, Chappellaz J, Raynaud D, Barnola JM (2002) High resolution Holocene N_2O ice core record and its relationship with CH_4 and CO_2. Glob Biogeochem Cycle 16: DOI 10.1029/2001GB001417

Fröhlich C, Lean J (2004) Solar radiative output and its variability: evidence and mechanisms. Astron Astrophys Rev 12:273–320

Ganopolski A, Kubatzki C, Claussen M, Brovkin V, Petoukhov V (1998) The Influence of Vegetation–Atmosphere–Ocean Interaction on Climate during the Mid-Holocene. Science 280:1916–1919

Gilli A, Anselmetti F, Ariztegui D, Beres M, McKenzie J, Markgraf V (2005a) Seismic stratigraphy, buried beach ridges and contourite drifts: the Late-Quaternary history of the closed Lago Cardiel basin, Argentina (49°S). Sedimentology 52:1–23

Gilli A, Ariztegui D, Anselmetti F, McKenzie J, Markgraf V, Hajdas I, McCulloch R (2005b) Mid-Holocene strengthening of the Southern westerlies in South America - Sedimentological evidences from Lago Cardiel, Argentina (49° S). Glob Planet Change 49:75–93

Haberzettl T, Fey M, Lücke A, Maidana N, Mayr C, Ohlendorf C, Schäbitz F, Schleser GH, Wille M, Zolitschka B (2005) Climatically induced lake level changes during the last

two millennia as reconstructed in sediments of Laguna Potrok Aike, southern Patagonia (Santa Cruz, Argentina). J Paleolimn 33:283–302

Hall A, Clement A, Thompson D, Broccoli A, Jackson C (2005) The Importance of Atmospheric Dynamics in the Northern Hemisphere Wintertime Climate Response to Changes in the Earth's Orbit. J Clim 18:1315–1325

Hurrell J, van Loon H, Shea D (1998) The mean state of the troposphere. In: Karoly D, Vincent DG (eds) The Meteorology of the Southern Hemisphere, Vol 49, American Meteorological Society, pp 1–46

Janowiak JE, Gruber A, Kondragunta CR, Livezey RE, Huffman GJ (1998) A comparison of the NCEP/NCAR reanalysis precipitation and the GPCP rain gauge-satellite combined dataset with observational error considerations. J Clim 11:2960–2979

Jenny B, Wilhelm D, Valero-Garcés B (2003) The Southern Westerlies in Central Chile: Holocene precipitation estimates based on a water balance model for Laguna Acuelo 33°50'S. Clim Dynam 20:269–280

Jones J, Widmann M (2003) Instrumental and Tree-Ring-Based Estimates of the Antarctic Oscillation. J Clim 16:3511–3524

Kistler R, Kalnay E, Collins W, Saha S, White G, Woollen J, Chelliah M, Ebisuzaki W, Kanamitsu M, Kousky V, van den Dool H, Jenne R, Fiorino M (2001) The NCEP/NCAR 50-year reanalysis: monthly means CD ROM and documentation. Bull Am Meteor Soc 82:247–267

Lamy F, Hebbeln D, Röhl U, Wefer G (2001) Holocene rainfall variability in southern

Chile: a marine record of latitudinal shifts of the Southern Westerlies. Earth Planet Sci Lett 185:369–382

Lean J, Rottman G, Harder J, Kopp G (2005) SORCE contributions to new understanding of global change and solar variability. Sol Phys 230:27–53

Legutke S, Voss R (1999) The Hamburg atmosphere-ocean coupled model ECHO - G. Tech. Rep. 18, German Climate Computer Center (DKRZ) (available online www.mad.zmaw.de/fileadmin/extern/documents/reports/ReportNo.18.pdf)

Li H, Ku T, Stott L, Anderson R (1997) Stable isotope studies on Mono Lake (californis). 1. d18O in lake sediments as proxy for climatic change during the last 150 years. Limnol Oceanogr 42:230–238

Lorenz DJ, Hartmann DL (2001) Eddy-zonal flow feedback in the Southern Hemisphere. J Atmos Sci 58:3312–3327

Lorenz S, Lohmann G (2004) Acceleration technique for Milankovitch type forcing in a coupled atmosphere-ocean circulation model: method and application for the Holocene. Clim Dynam 23:727–743

Luterbacher J, Xoplaki E, Dietrich D, Rickli R, Jacobeit J, Beck C, Gyalistras D, Schmutz C, Wanner H (2002) Reconstruction of sea level pressure fields over the Eastern North Atlantic and Europe back to 1500. Clima Dynam 18:545–561

Luterbacher J, Dietrich D, Xoplaki E, Grosjean M, Wanner H (2004) European seasonal and annual temperature variability, trends and extremes since 1500 A.D. Science 303:1499–1503

Mancini M, Paez M, Prieto A, Stutz S, Tonello M, Vilanova I (2005) Mid-holocene climatic variability reconstruction from pollen records (32° S–52° S). Quat Int 132:47–59

Mann M, Bradley R, Hughes M (1999) Northern Hemisphere temperatures during the past millennium: Inferences, uncertainities, and limitations. Geophys Res Lett 26:759–762

Markgraf V (1993) Paleoenvironments and paleoclimates in Tierra-del-Fuego and southernmost Patagonia, South-America. Palaeogeogr, Palaeoclimatol, Palaeoecol 102:53–68

Markgraf V, Bradbury J, Schwalb A, Burns S, Stern C, Ariztegui D, Anselmetti F, Stine S, Maidana N (2003) Holocene palaeoclimates of southern Patagonia: limnological and environmental history of Lago Cardiel, Argentina. Holocene 13:581–591

Masson V, Cheddadi R, Braconnot P, Joussaume S, Texier D (1999) Mid-Holocene climate in Europe: what can we infer from PMIP model-data comparisons? Clim Dynam 15:163–182

Matulla C, Groll N, Kromp-Kolb H, Scheifinger H, Lexer M, Widmann M (2002) Climate Change scenarios at Austrian National Forest Inventory sites. Clim Res 22:161–173

Mayr C, Fey M, Haberzettl T, Janssen S, Lücke A, Maidana N, Ohlendorf C, Schäbitz F, Schleser G, Struck U, Wille M, Zolitschka B (2005) Palaeoenvironmental changes in southern Patagonia during the last millennium recorded in lake sediments from Laguna Azul (Argentina). Palaeogeogr, Palaeoclimatol, Palaeoecol 228:203–227

Meneghini B, Simmonds I, Smith I (2006) Association between Australian rainfall and the Southern Annular Mode. Int J Climatol (in press)

Michaelson J (1997) Cross-validation in statistical climate forecast models. J Clim Appl Meteor 26:1589–1600

Mikolajewicz U, Scholze M, Voss R (2003) Simulating Near-Equilibrium Climate and Vegetation for 6000 Years BP. Holocene 13:319–326

Nakamura H, Shimpo A (2004) Seasonal variations in the southern hemisphere storm tracks and jet streams as revealed in a reanalysis dataset. J Clim 17:1828–1844

North G, Bell T, Cahalan R, Moeng F (1982) Sampling Errors in the Estimation of Empirical Orthogonal Functions. Mon Weather Rev 110:699–706

Rashid H, Simmonds I (2004) Eddy-zonal flow interactions associated with the Southern Hemisphere annular mode: Results from NCEP-DOE reanalysis and a quasi-linear model. J Atmos Sci 61:873–888

Reason CJC, Rouault M (2005) Links between the Antarctic Oscillation and winter rainfall over western South Africa. Geophys Res Lett 32: DOI 10.1029/2005GL022419

Renssen H, Goosse H, Fichefet T, Brovkin V, Driesschaert E, Wolk F (2005) Simulating the Holocene climate evolution at northern high latitudes using a coupled atmosphere-sea ice-ocean-vegetation model. Clim Dynam 24:57–69

Rind D, Shindell D, Perlwitz J, Lerner J, Lonergan P, Lean J, McLinden C (2004) The relative importance of solar and anthropogenic forcing of climate change between the Maunder Minimum and the Present. J Clim 17:906–929

Roeckner E, Arpe K, Bengtsson L, Christoph M, Claussen M, Dümenil L, Esch M, Giorgetta M, Schlese U, Schulzweida U (1996) The atmospheric general circulation model

ECHAM4: model description and simulation of present-day climate. Tech. Rep. 218, Max Planck Institut für Meteorologie

Schäbitz F (1999) Paläoökologische Untersuchungen an geschlossenen Hohlformen in den Trockengebieten Patagoniens. Tech. Rep. 17, Universität Bamberg

Silvestri E, Vera C (2003) Antarctic Oscillation signal on precipitation anomalies over southeastern South America. Geophys Res Lett 30: DOI 10.1029/2003GLO18277

Simmonds I, Keay K (2000) Mean Southern Hemisphere extratropical cyclone behavior in the 40-year NCEP-NCAR reanalysis. J Clim 13:873–885

Simmonds I, Wu X (1993) Cyclone behaviour response to changes in winter Southern Hemisphere sea-ice concentration. Q J R Meteorol Soc 119:1121–1148

Solanki S, Usoskin I, Kromer B, Schüssler M, Beer J (2004) Unusual activity of the Sun during recent decades compared to the previous 11,000 years. Nature 431:1084–1087

von Storch H, Zorita E, Cubasch C (1993) Downscaling of global climate change estimates to regional scales: an application to Iberian rainfall in wintertime. J Clim 6:1161–1171

Teranes J, McKenzie J, Bernasconi S, Lotter A, Sturm M (1999) A study of oxygen isotopic fractionation during bio-induced calcite precipitation in eutrophic Baldeggersee, Switzerland. Geochim Cosmochim Acta 63:1981–1989

Thompson D, Wallace J, Hegerl G (2000) Annular Modes in the Extratropical Circulation. Part II: Trends. J Clim 13:1018–1036

Thompson D, Baldwin M, Solomon S (2005) Stratosphere-troposphere coupling in the Southern Hemisphere. J Atmos Sci 62:708–715

Trenberth K (1982) Seasonality in southern hemisphere eddy statistics at 500 mb. J Atmos Sci 39:2507–2520

Trenberth K (1987) The zonal mean westerlies over the Southern Hemisphere. Mon Wea Rev 115:1528–1533

Villalba R, Cook E, Jacoby G, D'Arrigo R, Veblen T, Jones P (1998) Tree-ring based reconstructions of northern Patagonia precipitation since AD 1600. Holocene 8:659–674

Wardle R (2003) Using anticyclonicity to determine the position of the Southern Hemisphere westerlies: Implications for the LGM. Geophys Res Lett 30: DOI 2003GLO1879

Watkins A, Simmonds I (1995) Sensitivity of numerical prognoses to Antarctic sea ice distribution. J Geophys Res 100:22,681–22,696

Weber S, Crowley TJ, van der Schrier G (2004) Solar irradiance forcing of centennial climate variability during the Holocene. Clim Dynam 22:539–553

Widmann M, Bretherton C (2000) Validation of mesoscale precipitation in the NCEP reanalysis using a new grid-cell dataset for the northwestern United States. J Clim 13:1936–1950

Widmann M, Bretherton C, Salathés Jr EP (2003) Statistical precipitation downscaling over the northwestern United States using numerically simulated precipitation as a predictor. J Clim 16:799–816

Wolff J, Maier-Reimer E, Legutke S (1997) The Hamburg Primitive Equation Model

HOPE. Tech. Rep. 18, German Climate Computer Center (DKRZ)

Wyrwoll K, Dong B, Valdes P (2000) On the position of southern hemisphere westerlies at the Last Glacial Maximum: an outline of AGCM simulation results and evaluation of their implications. Quat Sci Rev 19:881–398

Yang S, Webster PJ (1990) The effect of summer tropical heating on the location and intensity of the extratropical westerly jet streams. J Geophys Res 95:18,705–18,721

List of Figures

List of Tables

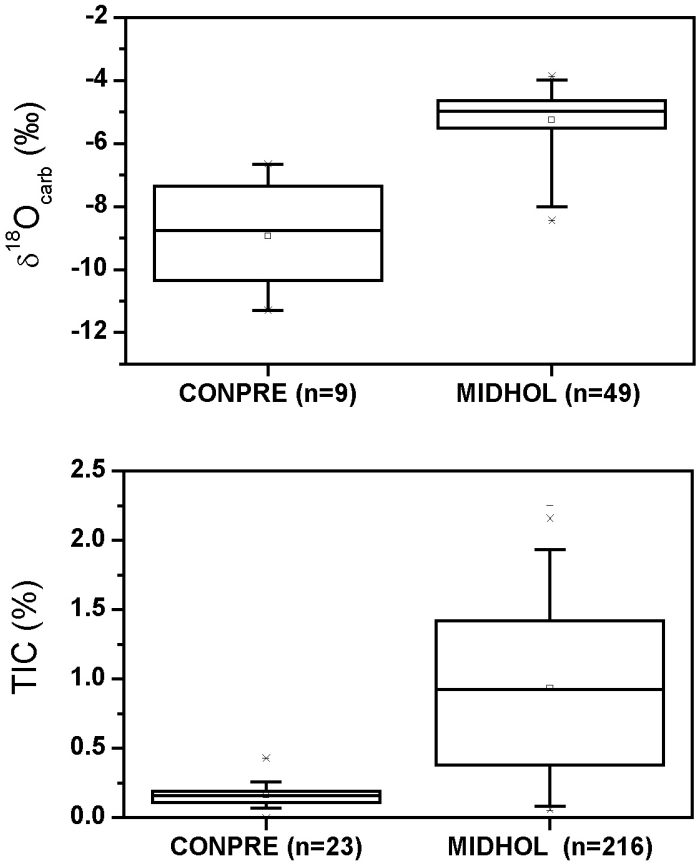

Figure 1: Proxies of Laguna Potrok Aike sediments related to lake level variations. Oxygen isotope composition of endogenic carbonates (δ^{18}Ocarb, upper panel) and concentration of total inorganic carbonates (TIC, lower panel) during the pre-industrial reference period (CONPRE; AD 1550–1850) and the middle Holocene (MIDHOL; 7.0–4.5 ka cal. BP) are given as box and whisker plots.

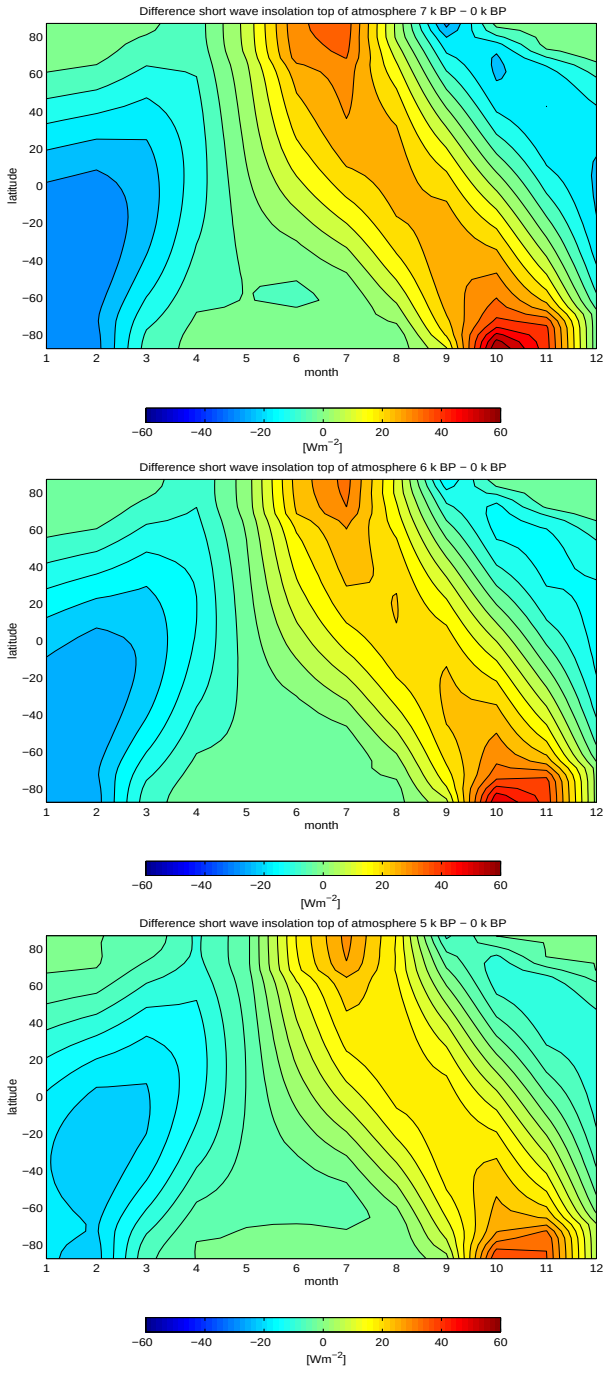

Figure 2: Insolation difference between different times of the mid-Holocene (7 ka, 6 ka, 5 ka BP) and present-day caused by changes in the orbital parameters.

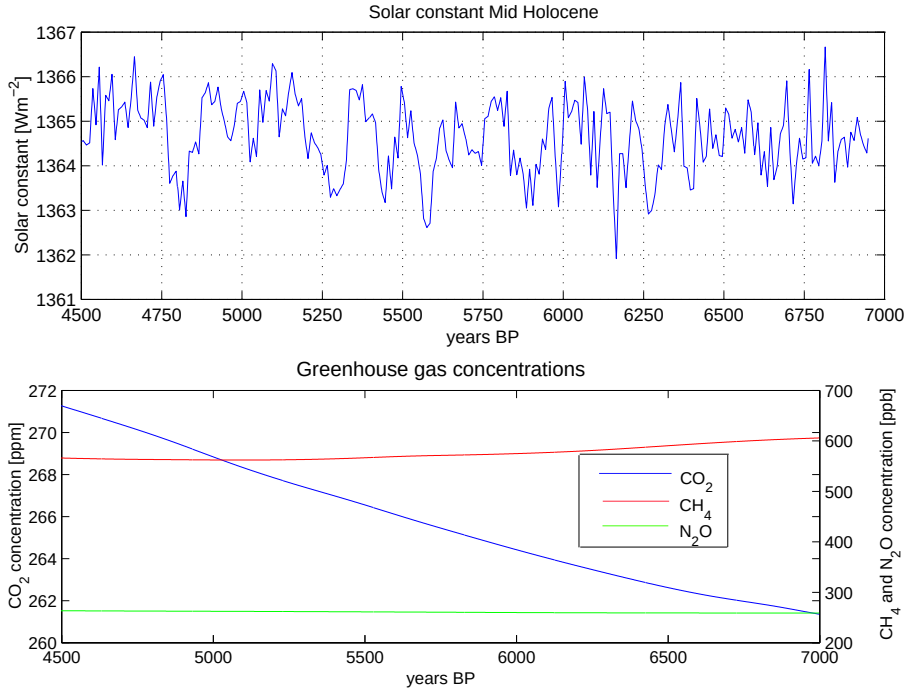

Figure 3: upper panel: Solar activity during the mid-Holocene based on production estimates of $\Delta\,^{14}C$ (Solanki et al., 2004). The curve has been scaled to an insolation difference between present-day and the Maunder-Minimum of 0.3% . Lower panel: Greenhouse gas concentrations derived from Antarctic ice cores (cf. Flückiger et al., 2002). These forcing time series have only been used for ORBSG. Note that the time axes runs from right to left.

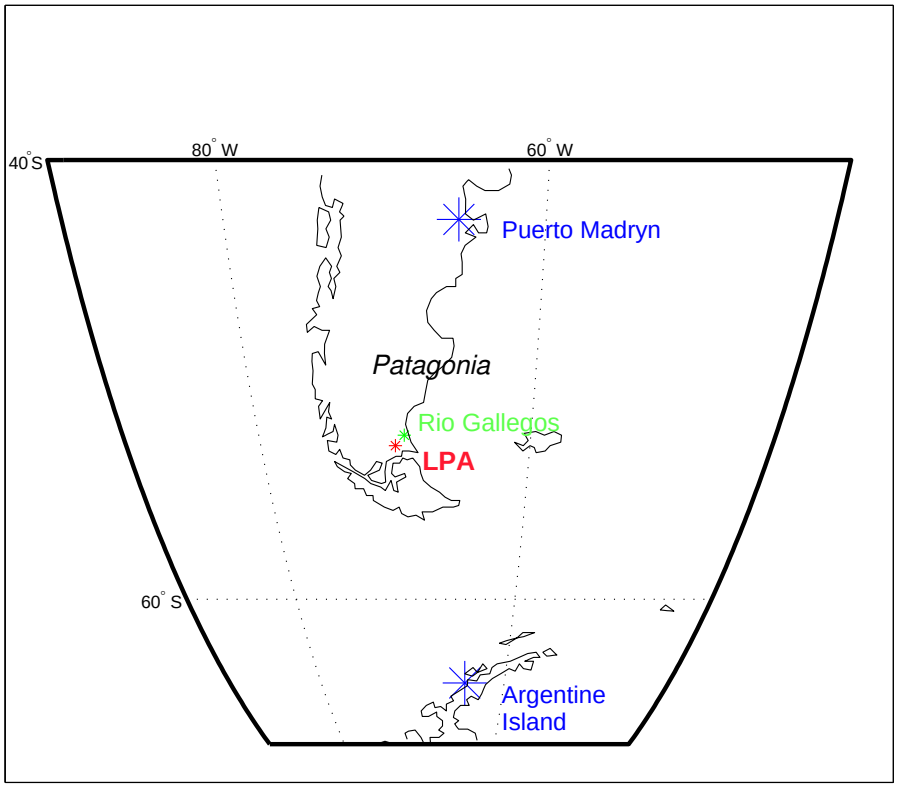

Figure 4: Location of the stations used to calculate the SAZI. The city of Rio Gallegos is located 90 km east of the Laguna Potrok Aike volcanic field (LPA).

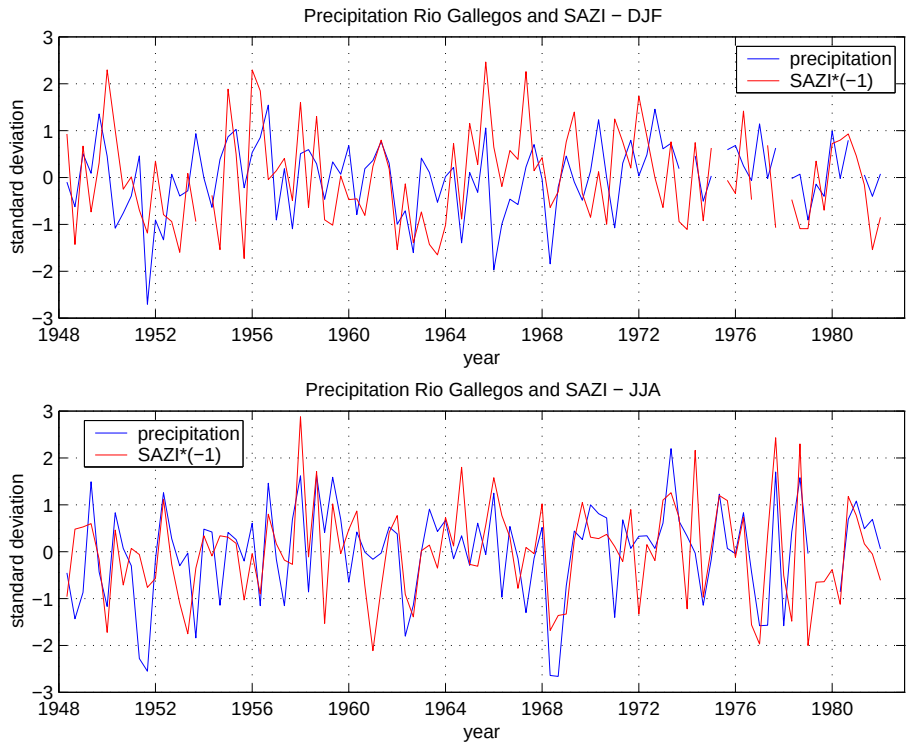

Figure 5: South American Zonal Index multiplied by -1 (SAZI, for definition see text) and standardised log-transformed precipitation anomalies at Rio Gallegos, south-eastern Patagonia during DJF (upper panel) and JJA (lower panel). Time series are correlated with r=-0.41 (DJF) and r=-0.56 (JJA).

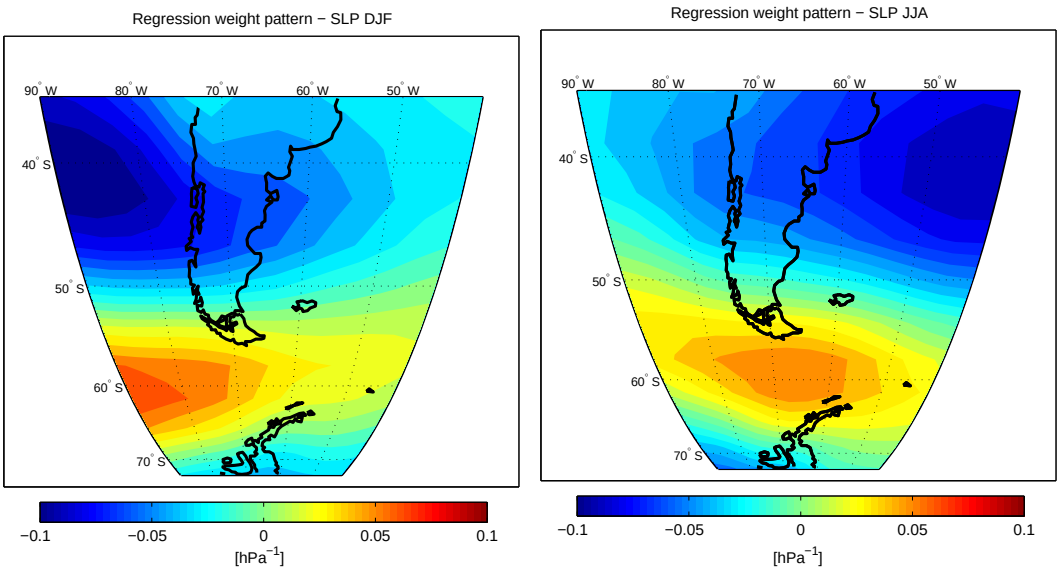

Figure 6: SLP regression weight patterns. left panel: DJF; right panel: JJA. Note the blocking-like structure that involves a reduction in the intensity of the southern extratropical westerlies.

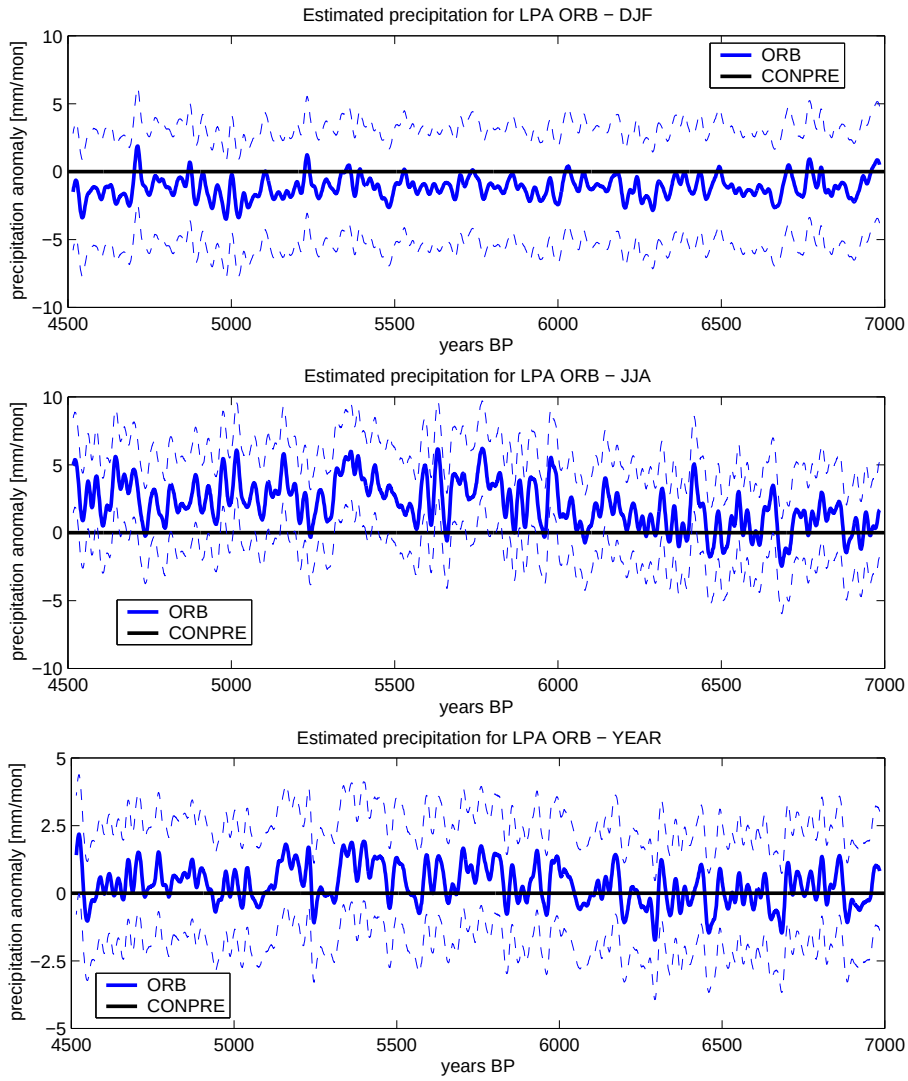

Figure 7: Estimated precipitation time series for the ORB simulation for the region of the LPA for DJF (upper panel), JJA (middle panel) and YEAR (lower panel). Time series have been smoothed with a 30 year Hamming window. The dashed lines indicate upper and lower 95% confidence intervals. The zero line indicates the mean of the pre-industrial simulation. Note the high uncertainty in the reconstruction indicated by the confidence intervals, especially during DJF. Note that the time axes runs from right to left.

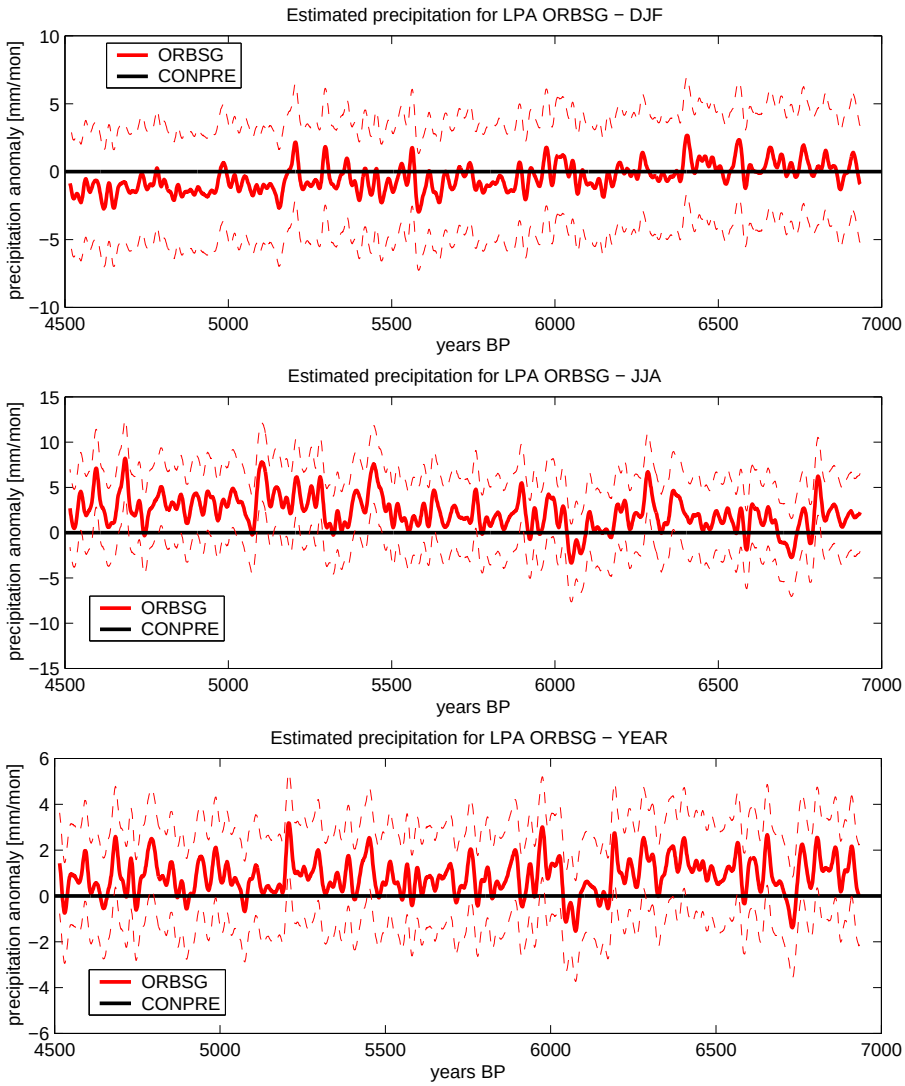

Figure 8: Same as Fig. 7, except for ORBSG. Note the positive trend during JJA. Note that the time axes runs from right to left.

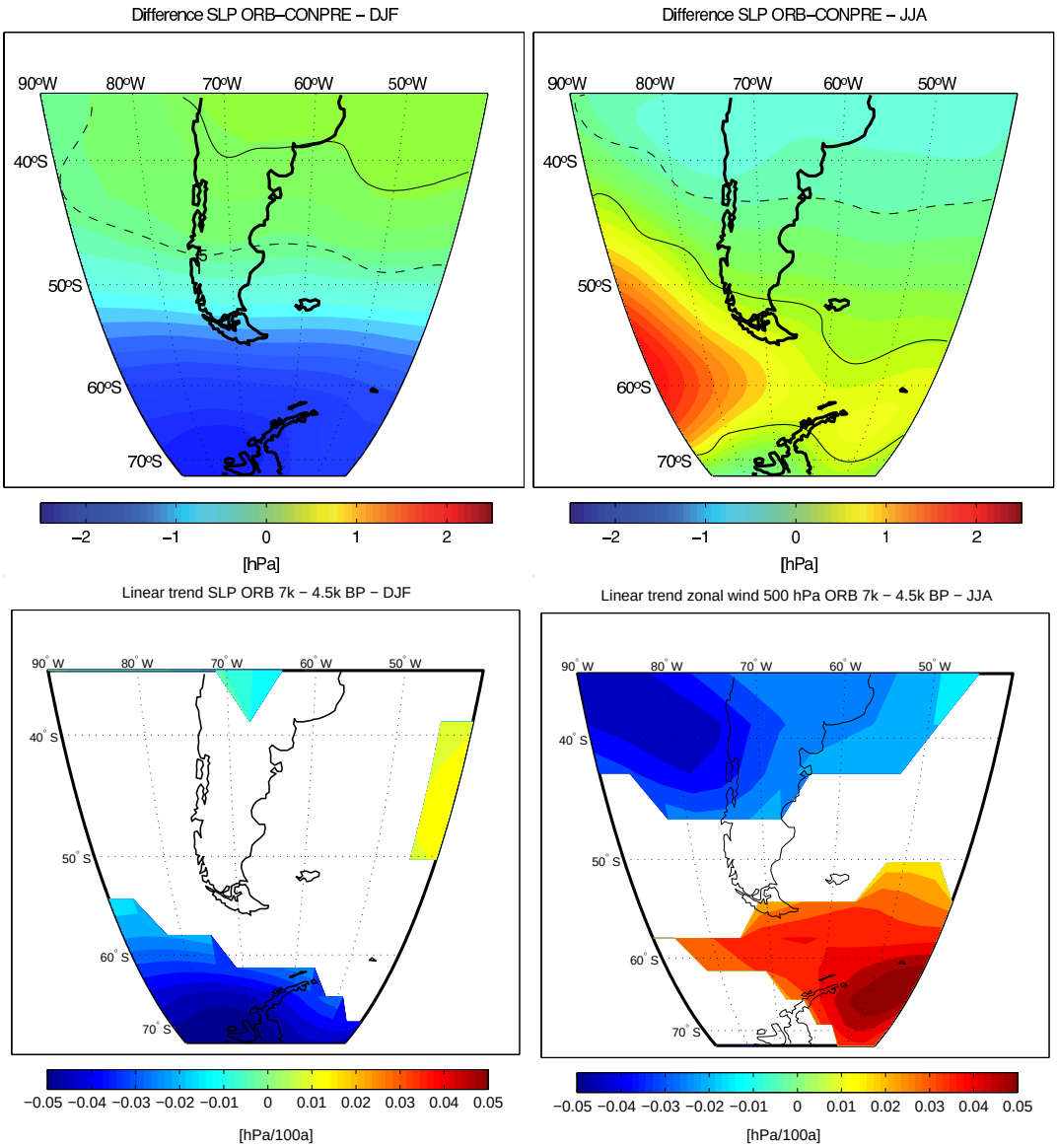

Figure 9: upper panel: SLP difference between ORB and CONPRE for DJF (left) and JJA (right); Black lines indicate statistical significance at the 5% level for negative (dashed) and positive (solid) differences according to a 2-sided t test. Note the reduced westerly flow over Patagonia during JJA and the increased westerly flow during DJF. lower panel: SLP trend in ORB for DJF (left) and JJA (right). Note the positive SLP trend in the JJA pattern extending into southern Patagonia.

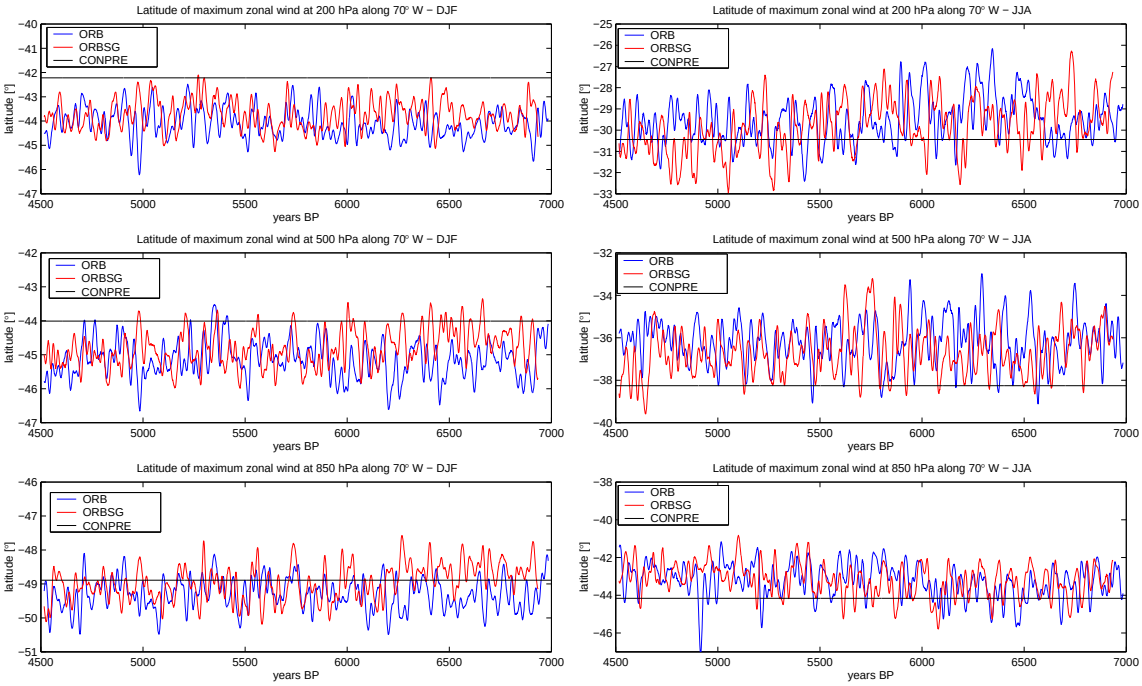

Figure 10: Latitude of maximum zonal winds (MZWs) along 70° W for DJF (left panel) and JJA (right panel) at the 200 hPa (upper panel), the 500 hPa (middle panel) and the 850 hPa level (lower panel). Time series have been smoothed with a 30 year Hamming window. Note the more poleward position of the MZWs during DJF and the more equatorward position of the MZWs during JJA. Note that the time axes runs from right to left.

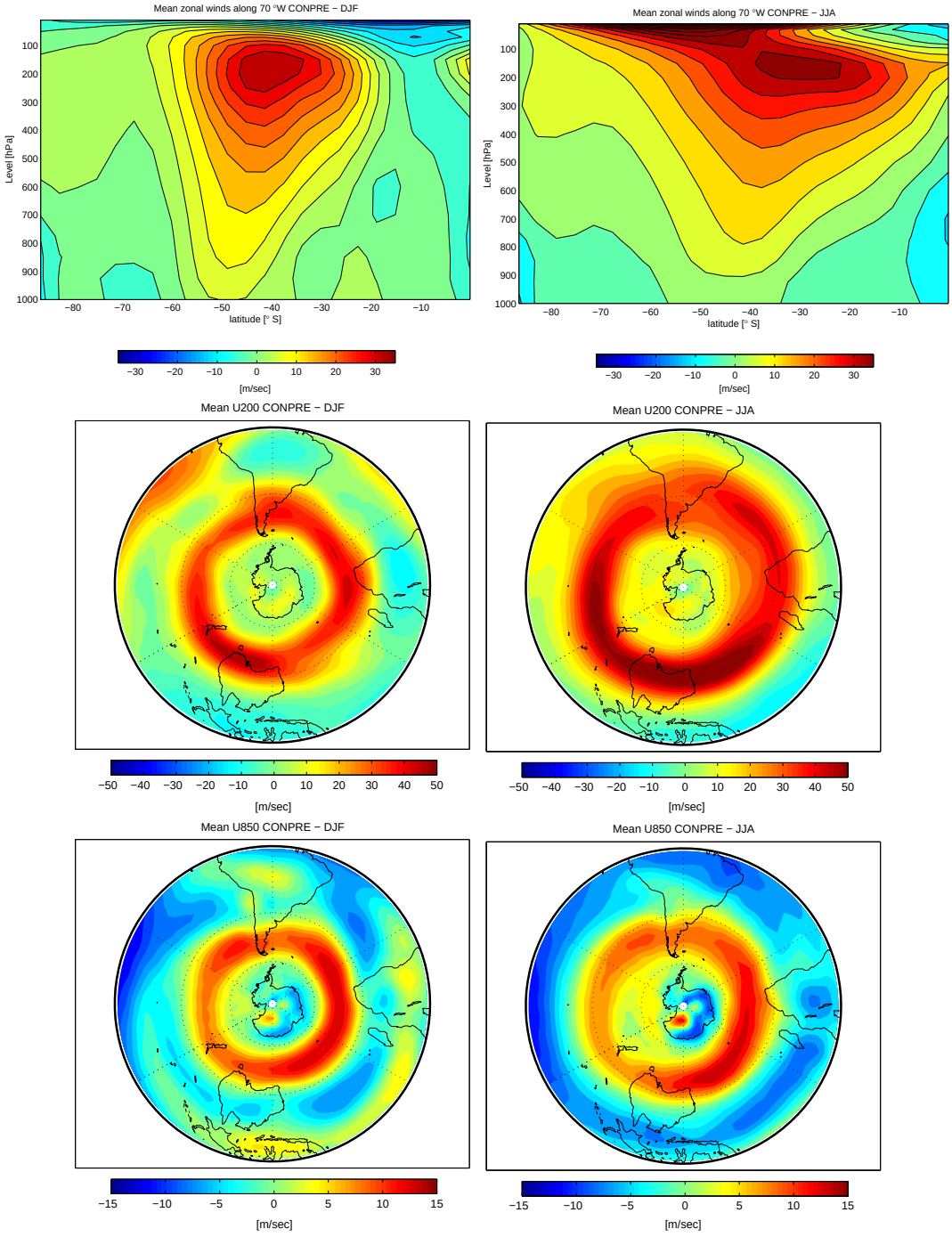

Figure 11: Mean zonal wind velocities along 70° W (upper panel) and for the Southern Hemisphere at the 200 hPa (middle panel) and 850 hPa level (lower panel) in CONPRE. Note the different position of the maximum zonal winds during DJF and JJA, respectively.

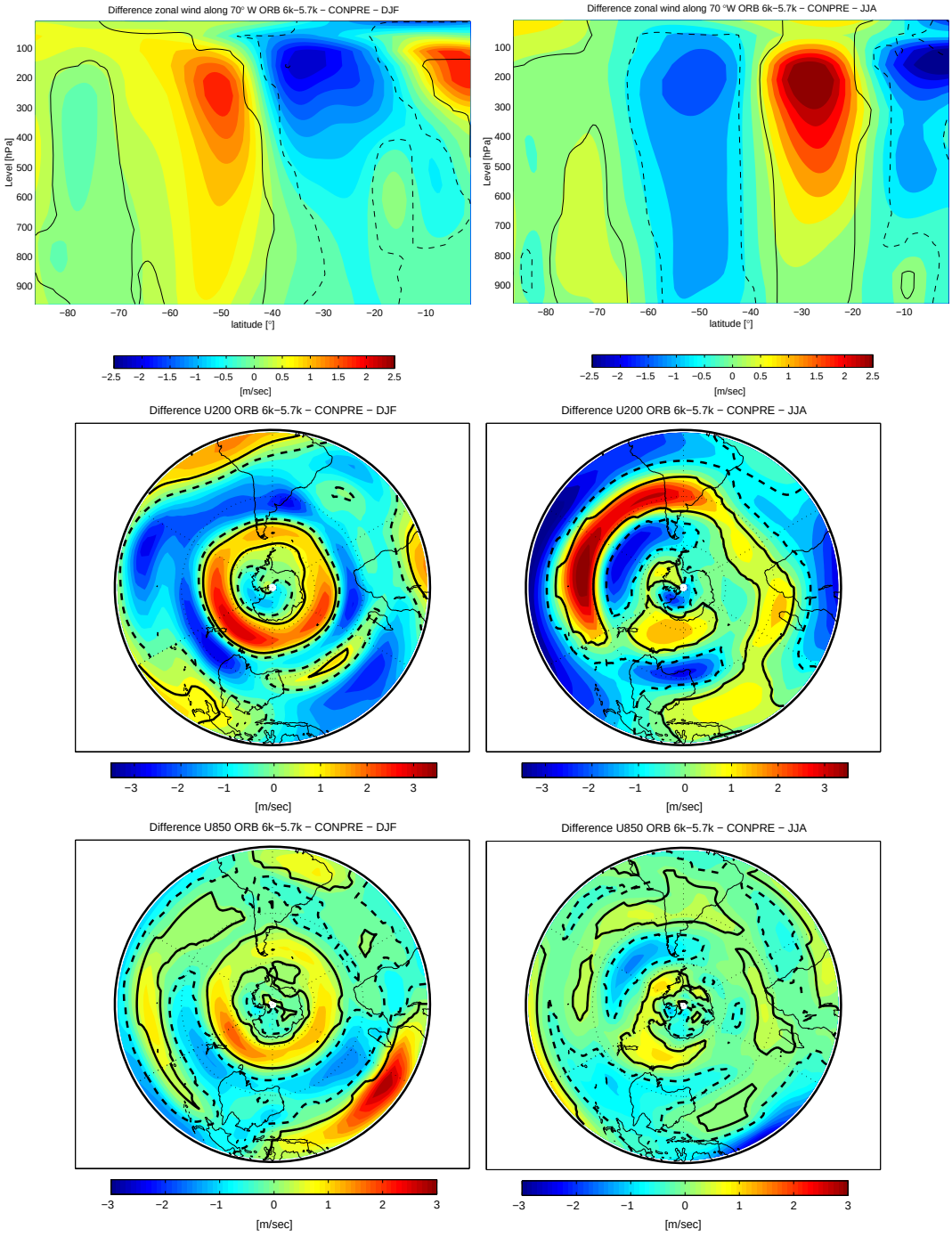

Figure 12: upper panel: Differences of zonal winds along 70° W between ORB (6 ka–5.7ka BP) and CONPRE; middle and lower panel: Differences of zonal winds for the Southern Hemisphere at the 200 hPa (middle panel) and 850 hPa level (lower panel); left panel: DJF; right panel: JJA; Black lines indicate statistical significance at the 5% level for negative (dashed) and positive (solid) differences according to a 2-sided t test. Note the narrowing and intensification of the southern jet during JJA during the mid-Holocene compared to pre-industrial conditions.

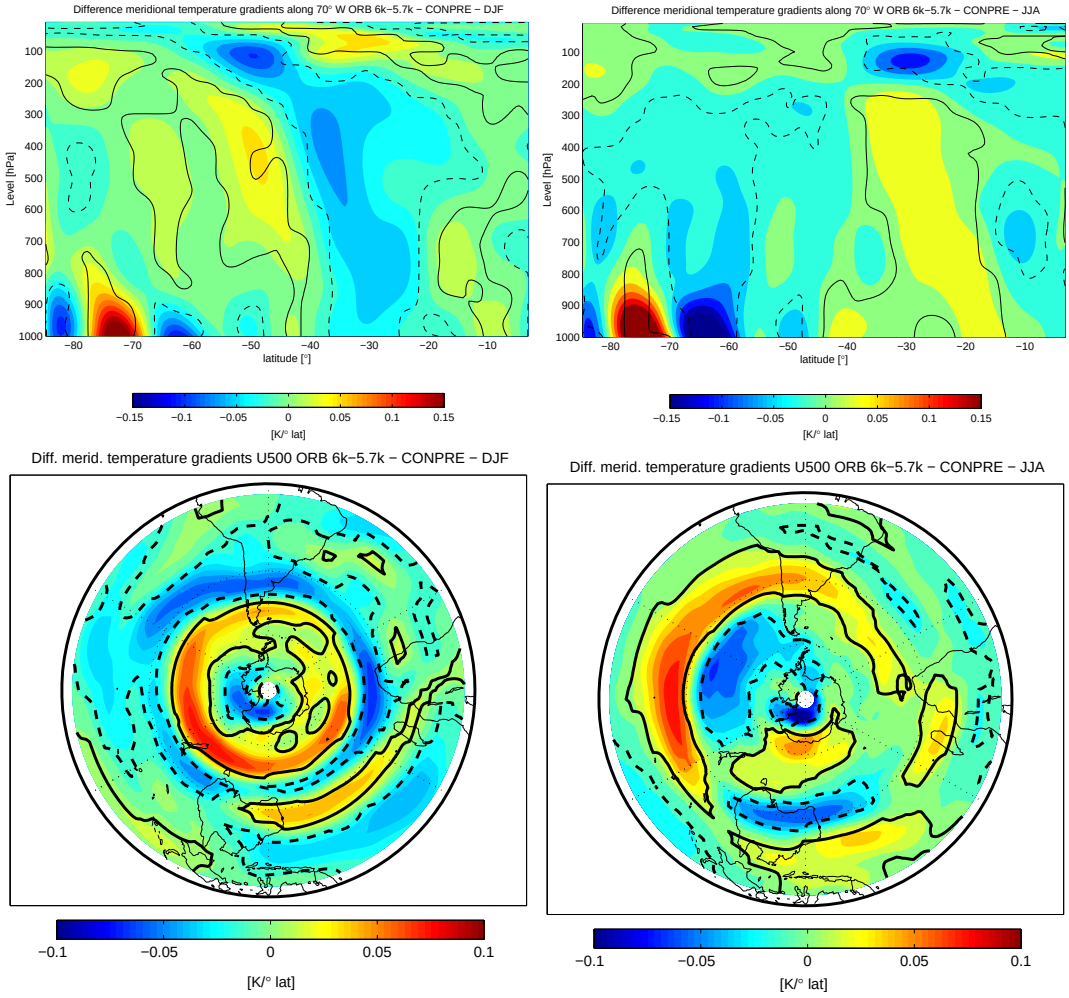

Figure 13: upper panel: Differences of meridional temperature gradients along 70° W between ORB (6 ka–5.7 ka BP) and CONPRE; lower panel: Differences of meridional temperature gradients at the 500 hPa level for the Southern Hemisphere; left panel: DJF; right panel: JJA; Black lines indicate statistical significance at the 5% level for negative (dashed) and positive (solid) differences according to a 2-sided t test. Note that regions with increased gradients are related to stronger winds and vice versa.

Season	r fitting all	r crossval	R.E. crossval	RMSE crossval
DJF	+0.37	+0.26	+0.06	16.0
MAM	+0.40	+0.35	+0.12	16.4
JJA	+0.49	+0.44	+0.19	17.2
SON	+0.42	+0.34	+0.11	14.8

Table 1: Skill measures for the multiple linear regression models used for the downscaling of the large-scale circulation. 1st col: Pearson correlation coefficients for whole fitting period; 2nd col: same as 1st except for the cross-validation period; 3rd col: Reduction in error; 4th col: root mean square error [mm/mon]. Note that the performance of the model is best in JJA. All correlations are statistically significant at the 1% level

Season	Mean VASCLIMO	ORB–CONPRE	ORBSG–CONPRE
DJF	32.93	–1.17 (–3.55)	–0.46 (–1.40)
MAM	34.28	+1.99* (+5.81)	+3.13* (+9.13)
JJA	29.70	+2.10* (+7.07)	+2.28* (+7.68)
SON	24.97	–1.66* (–6.64)	–1.53* (-6.13)
YEAR	30.47	+0.31 (+1.02)	+0.85 (+2.79)

Table 2: first column: Mean precipitation [mm/mon] at LPA (VASCLIMO); second and third column: Differences [mm/mon] for the estimated precipitation at LPA between the mid-Holocene simulations ORB and ORBSG and the pre-industrial simulation CONPRE. The values in parentheses denote the relative differences in % with respect to the mean of VASCLIMO at LPA in the period 1951–2000. The asterisk denotes statistical significance at the 5% level. The significance test is based on the observed twofold standard errors of the regression models.

	CONPRE	ORB	ORBSG
DJF			
200 hPa	42.22 [*35.38*]	44.09 (-1.87*) [*35.04 (-0.34)*]	43.74 (-1.52*) [*34.85 (-0.53*)*]
500 hPa	44.01 [*19.09*]	45.15 (-1.14*) [*19.83 (+0.74*)*]	44.82 (-0.81*) [*19.75 (+0.66*)*]
850 hPa	48.89 [*11.12*]	49.3 (-0.41)* [*11.84 (+0.72*)*]	48.96 (-0.07) [11.62 (+0.5*)]
JJA			
200 hPa	30.44 [*38.70*]	29.54 (+0.9*) [*41.12 (+2.42*)*]	29.8 (+0.64) [*40.25 (+1.55*)*]
500 hPa	38.26 [*19.65*]	36.21 (+2.05*) [*19.89 (+0.24)*]	36.69 (+1.57*) [*19.86 (+0.21*)*]
850 hPa	44.16 [*10.04*]	43.24 (+0.92)* [*9.63 (-0.41*)*]	43.17 (+0.99)* [*9.67 (-0.37*)*]

Table 3: Mean position (°S) [and *intensity* (m/sec)] of maximum zonal winds along 70° W. The difference to CONPRE is given in parentheses. Concerning the position '+' indicates a more equatorward position; '-' indicates a more poleward position in the mid-Holocene; The asterisk indicates values significantly different at the 5% level.